CHALMERS

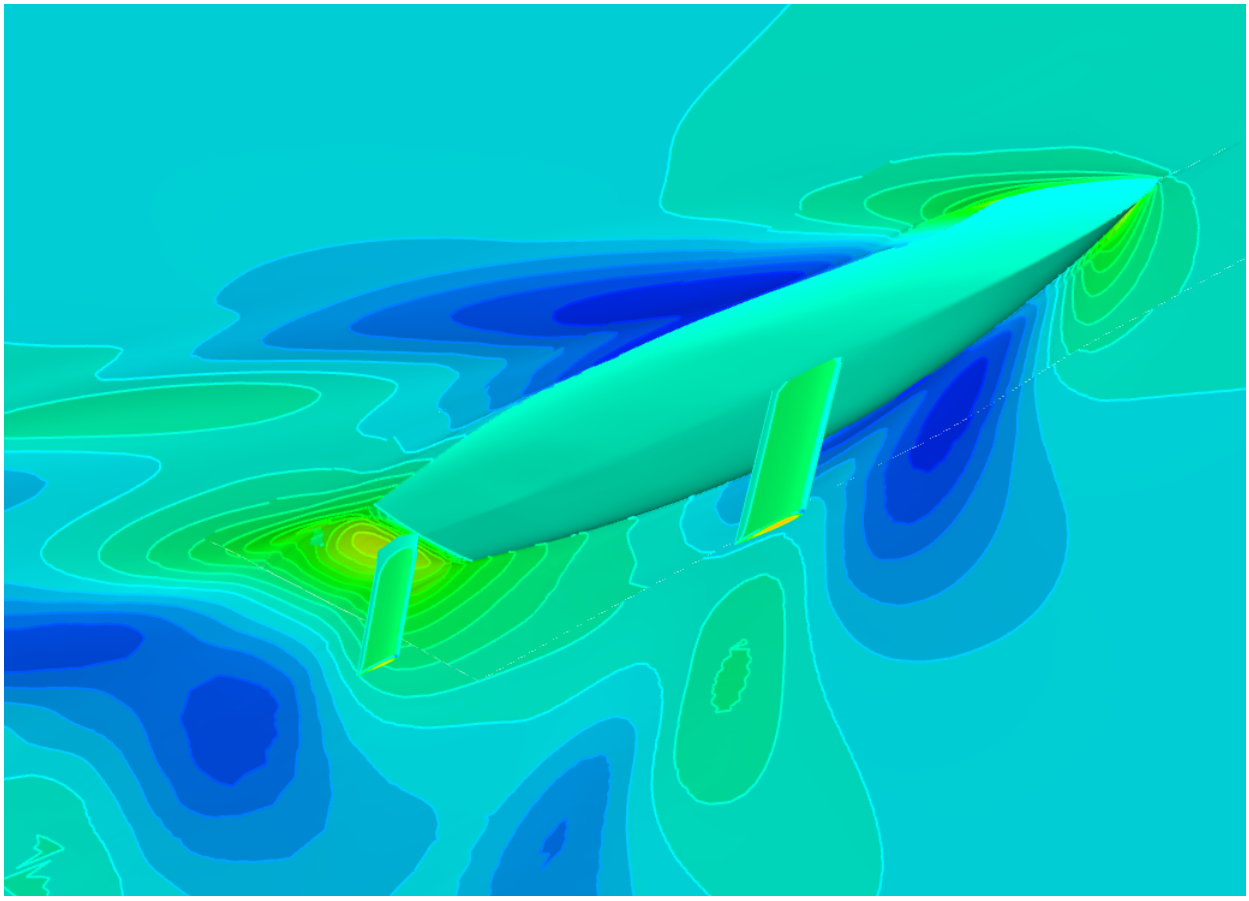

CFD prediction of the effect of heel and trim on the resistance of an Olympic dinghy

Master's of Science Thesis

RICKARD LINDSTRAND LEVIN

JEREMY PETER

Department of Shipping and Marine Technology
Division of Marine Design
CHALMERS UNIVERSITY OF TECHNOLOGY
Gothenburg, Sweden, 2014
Report No. X-14/304

A THESIS FOR THE DEGREE OF MASTER OF SCIENCE

CFD prediction of the effect of heel and trim on the resistance of an Olympic dinghy

RICKARD LINDSTRAND LEVIN
JEREMY PETER

Department of Shipping and Marine Technology
CHALMERS UNIVERSITY OF TECHNOLOGY
Gothenburg, Sweden 2014

CFD prediction of the effect of heel and trim on the resistance of an Olympic dinghy

RICKARD LINDSTRAND LEVIN
JEREMY PETER

Report No. X-14/304

Department of Shipping and Marine Technology
Chalmers University of Technology
SE-412 96 Gothenburg
Sweden
Telephone +46 (0)31-772 1000

Printed by Chalmers Reproservice
Gothenburg, Sweden, 2014

CFD prediction of the effect of heel and trim on the resistance of an Olympic dinghy

RICKARD LINDSTRAND LEVIN
JEREMY PETER
Department of Shipping and Marine Technology
Chalmers University of Technology

Abstract

Sailing the Laser dinghy will be an Olympic discipline at the 2016 summer Olympic Games in Rio. The Olympic motto reads: *Higher - faster - stronger*. For competitive sailing nowadays this means using scientific measures to improve boat speed and distance made good. This thesis is a part of Chlamers' *sports technology* effort which aims at improving of developing certain sports. This thesis in particular is undertaken in the aim at gaining insights on the parameters that affect the hydrodynamic resistance of the hull of the Laser dinghy. Gaining knowledge in how to minimize resistance will in turn provide the sailors with instructions of how to sail better. Investigations of this kind have never been done before on any dinghy, this increases the potential for an advantage for the Swedish sailors. As the Laser is a strict one-design class no means of design change is possible.

The overall goal of the sports project is to improve the performance of the sailors. The purpose of this thesis is to see if the minima in resistance can be predicted to occur at the same angles of heel and trim for: bare hull towing tank tests, bare hull simulations and appendage and leeway simulations. If this is the case the appendages and the leeway can be rejected from future investigations of this kind. This would be beneficial as they impose further complexity to the simulations. To get direct instructions of how to sail according to the results obtain in this thesis, more work than presented here is needed.

Towing tank tests performed at SSPA in Göteborg are the input and the starting point of this thesis. The test were performed for variations of speed and heel and trim angles, for a bare hull. In the first phase of the project, a verification and validation, V&V, analysis is achieved to gain confidence in the CFD simulations run in the Shipflow software. The verification is done to display and effect of the grid on the outcome of the simulation, the procedure is called grid dependence study. The V&V was done for one test case with 4 kts boat speed. The second part of the thesis work was to run simulations with similar conditions as in the towing tank and then validate the results against the towing tank test data. This was done for heel and trim variations at 3 and 4 kts. The third part was to include the effect of appendages and the leeway to the simulations, and then see if the resistance minima occurred for the same angles of heel and trim.

The results from the V&V study showed that the numerical method predicted a too low resistance. Possible sources of error were identified and systematically investigated but the major source of error was not found. However some possibilities are explained and ruled out for future reference. Furthermore, not all simulations for the investigation were finished or did not provide satisfactory and reliable results. Having an incomplete set of results, conclusions on the angles of heel and trim leading to minimal resistance could not be made. A discussion about what needs to be done in order to reach those objectives, and what could improve a study like this one in the future, is given in the end of this report.

Keywords: *Hydrodynamic resistance, CFD, Laser dinghy, Validation & Verification*

Preface

This thesis presents the work carried out at the Department of Shipping and Marine Technology at Chalmers University of Technology, during the spring semester of 2014. This thesis is submitted as a partial fulfillment for the degree of Master of Science.

We would like to thank our supervisors Prof. Lars Larsson and Michal Orych, for guiding, teaching and sharing knowledge with us during this work.

Contents

1

Introduction

This chapter will explain the starting point for this thesis and the background of the subject. It will also clarify why the sought results are of interest.

1.1 Context

This thesis is a part of the extra effort Chalmers has made into *sports and technology*. This new area of research is in turn is a part of one of Chalmers' areas of advance: *Material Technology*. This is a large project that includes many different participants from different levels of education and from all over Chalmers. The common factor for these projects is that the evolution of the sport at hand has to some extent been driven by introduction of new materials.

A common trend in sports overall is also the desire to use scientific measures to quantify and evaluate changes in techniques or equipment. This is interesting in sports where more or less drastic changes only give small results that are almost undetectable otherwise. This is why the national sport society wants to include a university in the pursuit of new records and future Swedish Olympic gold medals.

The sport of concern for this thesis is sailing, the Laser class dinghy in particular. The Laser dinghy will be an Olympic event during the 2016 Rio Summer Olympics, and is a class that Sweden will represent with a team of good sailors. The particulars of the dinghy will be described later on. As the hull of the dinghy has a complex three-dimensional shape the flow around it will differ for different attitudes to the direction of motion. This means that there is potential to find a minimum of the hydrodynamic resistance by sailing at a specific angle of trim and heel. This is the overall objective with this thesis; to contribute in providing the sailors with useful instructions on how to sail their dinghies in a way that minimizes resistance and thereby maximizes speed.

There are of course other effects than the hydrodynamic resistance to account for when the angle of heel and trim of the dinghy are changed. The projected area for the centerboard and rudder is decreased when the dinghy is heeled, and so for the sail. Also the stability could be decreased when trimming on the bow for example. The angles of heel and trim are changed by positioning the sailor in a certain way in the dinghy. This is possible to a large extent since the weight of the sailor represents amply half of the displacement.

As the forces acting on the dinghy at moderate speeds are small, only a slight change in resistance can result in a great advantage against the opponent sailors. On a professional level with similarly good sailors, possibilities like this must be exploited to gain the upper hand on the race course.

1.2 Background

The governing equations for the dynamics of a fluid are the Navier-Stokes equation, NS, and the continuity equation. Fully resolving the flow around a ship, yacht or dinghy with these equations is however not possible. This is due to the huge separation of scales in the domain and the computational effort required for handling this. The length of a ship can range from hundreds of meters to the 4 meters of the Laser dinghy, while the smallest scales in the flow, the Kolmogorov scales, are just a tiny fraction of a millimeter. This means that the resolution of the discretized domain needs to be incredibly fine in order to fully resolve the flow [6]. To resolve one of the smallest turbulent scales it takes approximately 4 cells in each spatial direction. Also to account for the fact these turbulent structures only live a very short period of time, the temporal resolution also needs to be great.

For ship applications the level of resolution must therefore be limited to result in a certain amount of cells that are considered to be affordable. Increasing the cell size leads to loss of information of the smaller turbulent structures. To make up for this loss of information turbulence models and near wall function are introduced to the simulation. The temporal resolution is neglected all together. The motivation for doing so is the fact that the average quantities of the flow is of greater interest than the instant ones [9]. For example it may be more valuable to know the average the hydrodynamic resistance, than the value at each hundreds of a second. A result of neglecting the temporal discretization is that the equations have to be adjusted to handle averaged quantities of pressure and velocities. This operation is called Reynolds time averaging, and the new equation is called the Reynolds time averaged Navier-Stokes equation, or simply RANS.

There are other methods based on even further simplifications for resolving flow around ships. However, as more simplifications are made more and more information about the details of the flow are lost.

In documentation available to the public it is evident that performing tests and simulations with the level of ambition aimed on in this thesis, on a sailing dinghy, has never been carried out before.

The reason why there is no trace of previous investigations of his type could be due to the fact that the results are to benefit only a certain group, the national sailing team for example, or the fact that the towing tank tests that is necessary for the validation are very expensive to perform. The computational fluid dynamics simulations, even simplified to the RANS method, for dinghies do also require considerable resources in term of computing power, which could also be a limiting factor. Projects with investigations like this one have been performed before, but only for large yachts for racing events requiring great amounts of sponsor funding. Such events have been the Americas Cup and the Volvo Ocean race for example. Other projects where fluid dynamics investigations have been made are luxury super yachts of sizes around 100 feet.

As investigations like this one have never been done before, the potential for an advantage for the Swedish sailors are good.

1.3 Aim

The aim with this thesis is foremost to investigate the effect of the leeway and appendages, on finding the attitude (angle of heel and angle of trim) generating the minimum amount of hydrodynamic resistance. As in the first towing tank tests, performed in the first days of 2014, the setup was rather simplified. First the appendages, the rudder blade and the centerboard, were not included in these tests. These appendages are in fact in the water for this dinghy for all kinds of sailing, both upwind and downwind. Second the inevitable leeway of a sailing craft was not taken into account either. The purpose of this thesis was to investigate if the minima of resistance can be found for the same angle of heel and trim for the case of leeway and appendages as for the case with bare hull and no leeway. If this would turn out to be true considerable savings in future investigations of this kind can be made. Indeed, the computational model for the case of no leeway is symmetric and therefore saves computational power. Also no special grids for the appendages have to be made which saves work.

1.4 The Laser dinghy class presentation

The Laser dinghy is an international one-design sailboat racing class. It is one of the most popular single-handed dinghies in the world. This dinghy presents very competitive racing due its very tight class association control.

History

The first Laser prototype was designed by Bruce Kirby and was unveiled in 1970 at an American regatta for boats under $1000. The boat easily won the regatta. The dinghy was originally named the "Weekender" at this time, when officially revealed at the following New York Boat Show in 1971 it was given the name it goes by today: "Laser".

The Laser class in the Olympic Games

The Laser is a challenging boat that rewards athleticism and sailing techniques. The boat is being protected by a strict one-design class rule which makes it possible to compare equally the sailors against their own abilities. As far as class rules go, Laser has one of the strictest. The Laser became a men's Olympic discipline at the 1996 Summer Olympics in Atlanta. Sailing was first contested as an Olympic sport at the 1900 Paris Games. The classes of boats that are competing at the Olympics have been evolving since then but the common factor being that boats are categorized into a strict one-design class based on similar weights and measurements. Sailing the dinghy as a competitive sport is also governed by a set of rules published by the International Sailing Federation (ISAF).

Design

The International Laser Class Association is the organization that sets the rules concerning the Laser's design. The philosophy of the association is to maintain one very strictly controlled design

in order to make sailing competitions a measure of the sailing skills rather than a technical modification competition. Hence, the class rules are written to prevent any changes to the boat design that might affect its performance. As having tight design controls, the Lasers are all built to the same specifications. The hull is 4.23 m long, with a waterline length of 3.81 m and a beam width of 1.37 m. The hull weight is 56.7 kg . Finally, the Laser Standard boat has one main sail of 7.06 m^2. The boat comprises a NACA 00 wing shaped centerboard and rudder.

1.5 Brief discussion on the mechanisms of sailing

Leeway is the term for the phenomenon of a sailing craft slightly translating to the leeward side as it is moving along. This phenomenon comes into play for upwind sailing, which is also for when this discussion is valid. During upwind sailing the sails are sheeted at small angles to the centerline, say 12^o, and the yacht has a true wind angle of roughly 45 degrees to the wind. From a fluid dynamics point of view, leeway results in that the flow will not be symmetrical along the centerline of the yacht.

The sail can be seen as a thin wing profile. The wing generates lift and drag, defined as force components perpendicular and parallel to the apparent wind respectively. The apparent wind is the wind that the sail experiences, i.e. with the boat velocity included (see figure 1.1).The point where the pressure field of the sail can be substituted by one force vector is called the center of effort. As the center of effort is dependent on the pressure distribution it is not trivial to find, but as an estimation it can be said that it is located in the surface center of the sail.

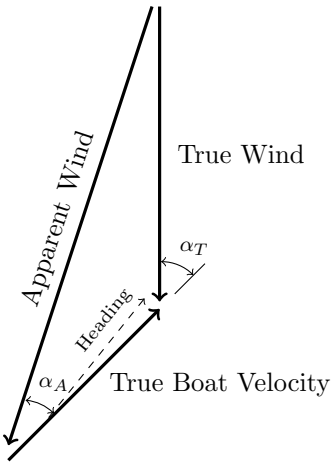

Figure 1.1: Working wind speeds and directions. The leeway is the difference between the heading and the true boat velocity.

The leeway, which will be a phenomenon of investigation in this thesis, is the result of that the total force vector of the sail is not aligned with the direction of motion of the yacht. In fact the largest part of the resulting force generated by the sail is forcing it to the side. And as the center of effort of the sail is not at the same height as the center of pressure for the hull and keel, a heeling moment will also be generated.

The lift of the sail is the only component acting in the positive direction of motion of the yacht and therefore the only component contributing to the propulsion. Furthermore only a component of

the lift is in turn completely aligned with the direction of the yacht. In order for the yacht to move in the right direction this driving force component has to balance: the hydrodynamic resistance of the hull, the component of the drag generated by the sail aligned with the opposite direction of the yacht and also the drag generated from the rigging and deck equipment etc.

1.6 Procedure

1.6.1 Overview

The goal for this thesis is to see if simulations can predict the minima in resistance for a Laser dinghy, for the same angles of heel and trim as the towing tank tests. To achieve this goal, first of all, the results of the simulations needed to be trusted. Therefore the thesis work started by doing a verification study. This was done by investigating how the error of the solution decreases with a systematic decrease in cell size. The verification procedure will display in what range the true value of the resistance can be expected to be. This will be further discussed in section 2.4.

Next step was a validation of the results from the simulations. By validation means comparing the results of the simulations to the results from the towing tank tests. I.e. the verification can be done without knowledge of the true value of the resistance, but the validation needs the test data. Also included in this procedure is to confirm that the results of the simulation end up in an acceptable error interval around the test results. For a thorough explanation of the validation procedure see section 2.5.

After the two first steps, acting as a confirmation that the code is correct tool for solving the flow of this particular application, the main investigation of the thesis was done. The purpose of the investigation was to see if adding appendages and leeway will predict the same force trend as the cases without. The results of the investigation and a complete set of the towing tank test data can be seen in the Result chapter.

A schematic view of the sub tasks done in this thesis work can be seen in the following figure:

1.6.2 Materials

The materials required for completing the work of this thesis will hereby be explained.

- **Rhinoceros 5** - This is a CAD software that was used for handling the geometry files. The geometry of the hull was scanned and some work was therefore required in order to make it more suitable for the meshing tool. Hydrostatic data for the hull was also obtained from the Orca extension in Rhinoceros.

- **Matlab 2013** - This is a mathematics and matrix handling software. It was used for the post processing to collect results and preparing the 2D plots. Also the calculations needed for the grid convergence study was carried out in Matlab.

- **Shipflow 5.1** - This is a CFD software that uses a set of structured and overlapping grids. It was used for all simulation during the thesis.

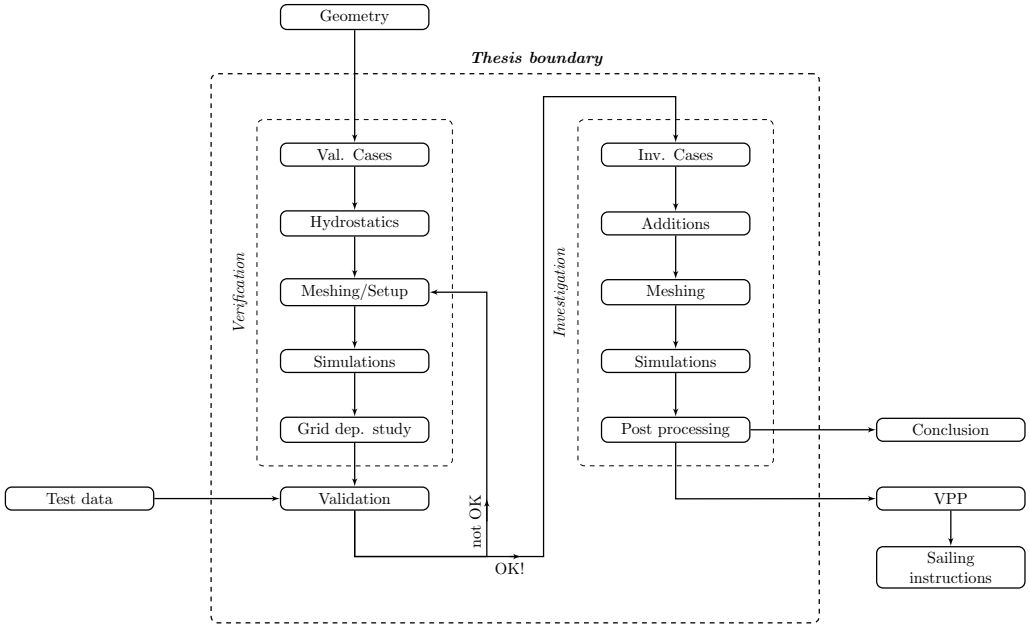

Figure 1.2: Thesis flowchart

- **Win scp** - This is a "secure copying program" that was used to transfer files to and from the PC-cluster Beda. The cluster was used for running the computationally demanding simulations that would have taken several times longer on an ordinary desktop.

1.6.3 Towing tank test setup

An advantage of testing a yacht with dimensions as small as the Laser is that the actual dinghy fits in the towing tank, the testing is done in full scale. The benefit of this is that there is no effect of erroneous scaling of the physical phenomena; viscosity, cavitation and surface tension. This in turn means that there is automatically similarity between the test case and the real case. If the testing model has to be scaled down the effects of scaling the viscosity, the surface tension and also the cavitation are sacrificed in order to keep the scaling of the gravitational effect similar. Strictly this means that the results of the model then cannot be scaled up in order to get the towing force of the full scale yacht.

These effects cannot all be satisfied as they do not scale in the same way, theoretically it can be achieved if the viscosity and density of the fluid in the towing tank could be arbitrarily selected. As this is not possible, fresh water is used in the towing tank. The gravitational effect is prioritized as it is the effect of most importance in the way the waves are created, and the fact that the effect of viscosity can be estimated by a flat plate analogy.

Some modifications were done to the dinghy in order to make it suitable for the towing tank tests. First an aluminum frame was fitted to the deck, around the cockpit. This frame provided a point to attach the towing device and also served to accommodate the weights that were used to position the dinghy in the desired heel and trim angles. Second the appendages were removed, to result in what will be called the *bare hull* case. The last modification was adding points to

attach string connected to measuring devices used to accurately measure the heel and trim during speed. As the dinghy in question was going to be used for sailing after the towing tank tests the hull could not be altered in any way. The test frame on the deck is displayed in the following figure.

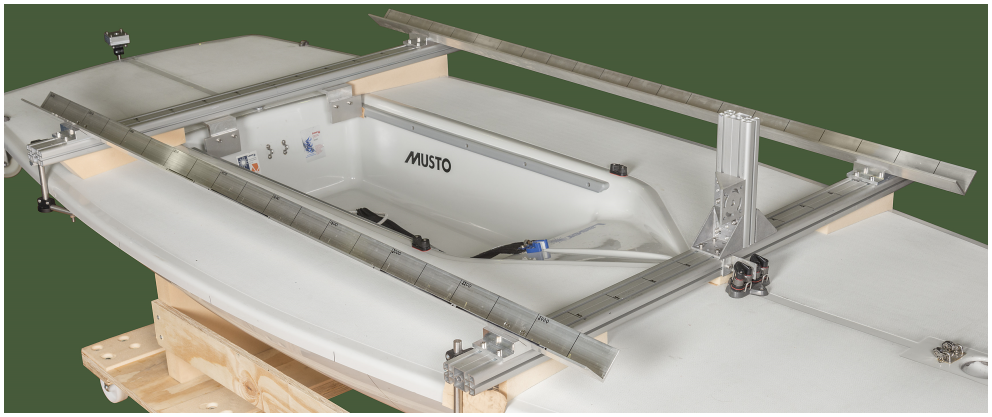

(a) Towing attachment and weight racks on deck.

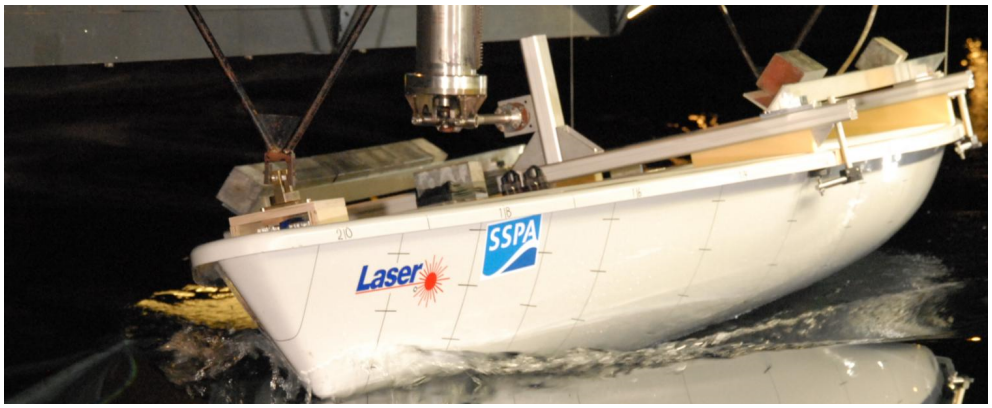

(b) Test setup during a run, loaded to an heel angle.

Figure 1.3: Display of the towing tank Laser.

At the top of the vertical aluminum profile is where the towing devise is attached. As the towing force is not applied through the center point of the hydrodynamic resistance, a trimming moment is hereby introduced. The arm of the towing devise was set up to be horizontal for the static cases. This meant that for the higher speeds when the dinghy had a considerable draft change, the arm would no longer be horizontal, and the towing force would pull the dinghy slightly downward. This will create an increase in displacement, which in turn will affect the resistance. Due to these facts the simulations that are to be performed could not be set to free sinkage and trim. The steel weights, representing the weight of the sailor, are to be securely placed in the v-profile racks on each side of the dinghy. Due to limited testing time the heel test were only preformed as heel to starboard. To add confidence to these tests a run at the same heel but to port side could be done, to make sure that the test setup was straight.

The brackets that are to some extent holding the frame in place are located on the railing of the dinghy, as can be seen in figure 1.3b. As the heel angle increased the ones on the starboard side were interfering with the spray from the bow wave. They were therefore removed from that side

and the test rerun. Despite this, luckily the frame stayed fixed to the deck!

During the test runs there was a bailing pump located on the flooring of the small cockpit. This was added to ensure that there was no excess water in the cockpit. The excess water originated from the self bailer device that was not completely water tight. Also the fact that the test setup was reversed back to the starting position in the towing tank, after each run, makes the self bailer leak.

1.7 Limitations

In time the Chalmers sailing project will extend to treat all the Olympic sailing classes, this thesis however, will only treat the Laser dinghy.

In the validation part of the thesis only the turbulence models included in the selected CFD software will be tested. As it was of interest to validate the code for this type of test case, no other software was considered. As the Shipflow software is normally used for motorized cargo ships which have a very different type of hull shape compared to a dinghy, this is of interest.

All of the towing tank tests were done using one single force measurement device. This means that there is a possibility of having false measurements for the validation procedure. To strengthen the argument that the force measuring device is accurate, the same test setup could be run at another test facility or using another device. The measurements are for this thesis considered to be accurate. As it was not in the scope of this thesis to confirm the measurements they shall however be viewed with caution.

During the towing tank tests, the heel and trim angles were induced by setting weights onto the boat. The measured resulting angles were recorded. The CFD simulations are run at fixed heel and trim angles in such a way that it matches with the measured angles from the towing tank tests. This is done so the results from the CFD simulations can be compared to the results from the towing tank tests. Consequently, no other angles are investigated in this project than the ones that were recorded during the towing tests.

2

Theoretical Background

2.1 Computational Method

2.1.1 Governing Equations

The governing equations of the fluid flow are derived from basic physical principles and described by the mathematical statements of the conservation law of physics, which are the conservation of mass and momentum. The Navier-Stokes equations are derived from the conservation laws with several underlying assumptions. They are used in naval architecture to model the flow of water around the hull of a moving ship and allow the designers to predict the resistance forces coming from the water pressure and viscous effects.

In the following section, the derivation of the governing equations is shown by first presenting the coordinate system and the basic assumptions. Then the continuity equation and the Navier-Stokes equations are derived.

Coordinate system

A few words deserve to be put in about the coordinate system used when dealing with yachts. In this thesis the yacht is assumed to have constant speed, the water surface is also assumed to be flat. For this reason, the coordinate system used is fixed to the ship. The simulations are thus set up not to account for changes in sinkage or trim. This is done because of the unnatural trimming moment and vertical force component created by the towing device, mentioned in section 1.6.3. A global Cartesian coordinate system is used in which the origin is at the bow on the centerline at the undisturbed water level and where x is directed sternward, y to starboard and z vertically upward. In this configuration, the water is considered as an inflow from ahead.

Basic assumptions

Several assumptions are made to simplify the process of mathematically modeling the fluid flow. Firstly, the Navier-Stokes equations are based on the assumptions that the fluid is a continuum meaning that the fluid is thought to be a continuous substance instead of being made up of discrete particles.

Commonly when dealing with water, the flow is considered incompressible. This implies that the density variation is not linked to pressure, making the density ρ and the viscosity μ constant.

In the next few paragraphs the main governing equations used to model the flow around the hull of a boat are presented. The assumptions described above are then taken into account.

The Continuity Equation

The velocities in the three spatial directions are hereby called: $u,\ v,\ w$, for the x-, y- and z- direction respectively.

If an infinitesimal fluid element $dxdydz$ is considered in a flow with no source of mass, the mass conservation equation or continuity equation can be derived simply. Assuming the mass flow follows the x-direction, it is the u-component that transports any mass in the system and through the surfaces of the fluid element. The mass inflow is then $\rho udydz$ and the outflow is $\left[\rho u + \frac{\partial}{\partial x}\rho u dx\right] dydz$. The net outflow in this direction is then $\frac{\partial}{\partial x}\rho u dxdydz$. Similar terms can be computed for the y and z directions.

Since there is no source of mass in the system, the total net transport of mass out of the element is null:

$$\frac{\partial}{\partial x}\rho u dxdydz + \frac{\partial}{\partial y}\rho v dxdydz + \frac{\partial}{\partial z}\rho w dxdydz = 0 \tag{2.1}$$

As stated earlier, the water is assumed incompressible and that enables to simplify the previous equation into the continuity equation for incompressible flows:

$$\frac{\partial u}{\partial x} + \frac{\partial v}{\partial y} + \frac{\partial w}{\partial z} = 0 \tag{2.2}$$

The Navier-Stokes Equations

The Navier-Stokes equations are derived by first applying Newtons second law to a fluid element $dxdydz$:

$$d\mathbf{F} = dm * \mathbf{a} = dm * \frac{d\mathbf{u}}{dt} \tag{2.3}$$

It is important to note that $\mathbf{u}$ in equation 2.3 is the velocity vector with a component in each direction that includes x,y and z but also a time component t. Therefore in the x-direction for example $\frac{du}{dt} = \frac{\partial u}{\partial t} + u\frac{\partial u}{\partial x} + v\frac{\partial u}{\partial y} + w\frac{\partial u}{\partial z}$. Similarly $\frac{d\mathbf{u}}{dt}$ is derived in the y and z directions.

The total force $\mathbf{F}$ on the element consists of the sum of the pressure forces F_P, the body forces F_b and the viscous forces F_v.

Including the three types of forces into the equation 2.3 and the following equality is obtained:

$$\frac{d\mathbf{u}}{dt} = \frac{d\mathbf{F_P}}{dm} + \frac{d\mathbf{F_b}}{dm} + \frac{d\mathbf{F_v}}{dm} \tag{2.4}$$

The three forces can be expressed in more details. The pressure force F_P, as it is expressed in vector form above, can be written in each of the three directions in which it acts on the element:

$$dF_{P_x} = -\frac{\partial P}{\partial x} dxdydz \tag{2.5}$$

Therefore when dividing by the unit mass: $\frac{dF_{P_x}}{dm} = -\frac{1}{\rho}\frac{\partial P}{\partial x}$.

Similarly, $\frac{dF_{P_y}}{dm} = -\frac{1}{\rho}\frac{\partial P}{\partial y}$ and $\frac{dF_{P_z}}{dm} = -\frac{1}{\rho}\frac{\partial P}{\partial z}$.

The body forces include forces proportional to the mass, for example: gravity, centrifugal force, Coriolis force and electromagnetic force. The only one that is reasonable to consider in this thesis is the gravity which acts in the negative z direction. Therefore the body forces can be expressed directionally as follow:

$$\frac{dF_{b_x}}{dm} = \frac{dF_{b_y}}{dm} = 0 \tag{2.6}$$

and

$$\frac{dF_{b_z}}{dm} = -g \tag{2.7}$$

The third category of forces is the viscous forces that are due to the shear stresses on the sides of the fluid element. The viscous forces terms are summed by adding up the stresses applied to the sides of the fluid element $dxdydz$. The total force due to viscous stresses per unit volume on the fluid expressed in each direction is:

$$\frac{dF_{v_x}}{dm} = \frac{1}{\rho}\left[\frac{\partial \tau_{xx}}{\partial x} + \frac{\partial \tau_{yx}}{\partial y} + \frac{\partial \tau_{zx}}{\partial z}\right] \tag{2.8}$$

$$\frac{dF_{v_y}}{dm} = \frac{1}{\rho}\left[\frac{\partial \tau_{xy}}{\partial x} + \frac{\partial \tau_{yy}}{\partial y} + \frac{\partial \tau_{zy}}{\partial z}\right] \tag{2.9}$$

$$\frac{dF_{v_z}}{dm} = \frac{1}{\rho}\left[\frac{\partial \tau_{xz}}{\partial x} + \frac{\partial \tau_{yz}}{\partial y} + \frac{\partial \tau_{zz}}{\partial z}\right] \tag{2.10}$$

The assumption that the fluid is Newtonian is convenient when modeling the viscous stresses. In a Newtonian fluid the viscous stresses are proportional to the local rate of deformation. This is expressed as the strain rate tensor: $S_{ij} = \frac{\partial u_i}{\partial x_j} + \frac{\partial u_j}{\partial x_i}$. The tensor consists of three linear strain components S_{xx}, S_{yy}, S_{zz} and six other components of the volumetric deformation rate [18]. The viscous stresses are linearly proportional to the strain tensor: $\tau_{ij} = \mu S_{ij}$ [9].

Hence the nine viscous stress components existing in the equations 2.8, 2.9 and 2.10 can be expressed in the following way:

$$\begin{aligned}
\tau_{xx} &= 2\mu\frac{\partial u}{\partial x} \\
\tau_{yy} &= 2\mu\frac{\partial v}{\partial y} \\
\tau_{zz} &= 2\mu\frac{\partial w}{\partial z} \\
\tau_{xy} = \tau_{yx} &= \mu\left(\frac{\partial u}{\partial y} + \frac{\partial v}{\partial x}\right) \\
\tau_{xz} = \tau_{zx} &= \mu\left(\frac{\partial u}{\partial z} + \frac{\partial w}{\partial x}\right) \\
\tau_{yz} = \tau_{zy} &= \mu\left(\frac{\partial v}{\partial z} + \frac{\partial w}{\partial y}\right)
\end{aligned} \tag{2.11}$$

The three types of forces, pressure forces F_P, body force F_b and viscous forces F_v are now defined. When put together, along with substituting the viscous stresses by their expressions stated in 2.11, the Navier-Stokes equations for incompressible flow are constituted.

In the x-direction:

$$\frac{\partial u}{\partial t} + u\frac{\partial u}{\partial x} + v\frac{\partial u}{\partial y} + w\frac{\partial u}{\partial z} = \frac{1}{\rho}\left[\frac{\partial^2 u}{\partial x^2} + \frac{\partial^2 u}{\partial y^2} + \frac{\partial^2 u}{\partial z^2} - \frac{\partial P}{\partial x}\right] \tag{2.12}$$

In the y-direction:

$$\frac{\partial v}{\partial t} + u\frac{\partial v}{\partial x} + v\frac{\partial v}{\partial y} + w\frac{\partial v}{\partial z} = \frac{1}{\rho}\left[\frac{\partial^2 v}{\partial x^2} + \frac{\partial^2 v}{\partial y^2} + \frac{\partial^2 v}{\partial z^2} - \frac{\partial P}{\partial y}\right] \tag{2.13}$$

In the z-direction:

$$\frac{\partial w}{\partial t} + u\frac{\partial w}{\partial x} + v\frac{\partial w}{\partial y} + w\frac{\partial w}{\partial z} = \frac{1}{\rho}\left[\frac{\partial^2 w}{\partial x^2} + \frac{\partial^2 w}{\partial y^2} + \frac{\partial^2 w}{\partial z^2} - \frac{\partial P}{\partial z}\right] - g \tag{2.14}$$

Note the gravity component in the Navier-Stokes equation 2.14 is due to the assumption that gravity is the only body force. An additional note can be made about the pressure term P. The pressure in an unsteady liquid is composed of two parts, the hydrostatic pressure P_{hs} that increases proportionally with the depth, and the hydrodynamic pressure P_{hd}. In the set of equations above the pressure P is sum of P_{hd} and P_{hs}. Hence $P_{hd} = P - P_{hs} = P + \rho g z$ and finally,

$$\frac{dF_{P_z}}{dm} + \frac{dF_{b_z}}{dm} = -\frac{1}{\rho}\frac{\partial P}{\partial z} - g \Rightarrow -\frac{1}{\rho}\frac{\partial\left(P + \rho g z\right)}{\partial z} \Rightarrow -\frac{1}{\rho}\frac{\partial P_{hd}}{\partial z} \tag{2.15}$$

In the x and y direction, $\frac{\partial P}{\partial x} = \frac{\partial P_{hd}}{\partial x}$ and $\frac{\partial P}{\partial y} = \frac{\partial P_{hd}}{\partial y}$. Replacing the total pressure P with the hydrodynamic pressure P_{hd} allows to cancel the gravity term in the z-component of the Navier-Stokes equations.

2.2 Turbulence

Turbulent flow

Typically, the fluid flow around the hull of a moving ship is turbulent. Turbulent flows are irregular, random and 3-dimensional. In turbulent flows the velocity and the pressure change continuously with time creating a spectrum of turbulent structures in the flow. Even though a turbulent flow is irregular, it is possible to resolve its behavior with the Navier-Stokes equations[1]. However the requirement of doing so is that the spatial and temporal discretizations are able to capture all scales in the flow. This is not possible for ship applications as the smallest scales are very small in comparison to the length of the hull, and this in turn leads to unreasonable computational effort.

To solve the turbulent flow that is present in the cases in this thesis, the Reynolds-averaged Navier-Stokes equation, RANS, is used. This means that the regular Navier-Stokes equations, presented in the previous section, are averaged over time. This is done by decomposing the instantaneous variables into a mean value $\bar{\phi}$ and a fluctuating value ϕ':

$$\begin{aligned} u_i &= \bar{U}_i + u_i' \\ P &= \bar{P} + p' \end{aligned} \tag{2.16}$$

Inserting the decomposed terms from 2.16 into the Navier-Stokes equations gives rise to the Reynolds-averaged Navier-Stokes (RANS) equations. For the incompressible Newtonian fluid, its expression in the Einstein notation is:

$$\frac{\partial \bar{U}_i}{\partial t} + \frac{\partial \bar{U}_i \bar{U}_j}{\partial x_j} = -\frac{1}{\rho}\frac{\partial \bar{P}}{\partial x_i} + \frac{\partial}{\partial x_j}\left[\nu\left(\frac{\partial \bar{U}_i}{\partial x_j} + \frac{\partial \bar{U}_j}{\partial x_i}\right) - \overline{u_i' u_j'}\right] \tag{2.17}$$

This is done in order to focus more on the mean values rather than the time histories because when solving the Navier-Stokes equations, a very fine resolution in time would be necessary to resolve the unsteady turbulent flow [1].

2.2.1 Modelling Turbulence

In the equation 2.17 the term $\overline{u_i' u_j'}$ appears from the fluctuating values. This term is called the Reynolds stress tensor. It is an unknown stress term that rises due to turbulences. In order to close the equation system and solve for all the unknowns, modeling the Reynolds stress tensor is needed. This is commonly called the closure problem [1].

There are many different ways to model the Reynolds stress tensor: algebraic models, one-equation models, two-equation models, algebraic stress models and Reynolds stress models. Each of these turbulence models varies in terms of computational requirement, accuracy in modeling the turbulence and complexity.

In this thesis, two turbulence models have been tried out in Shipflow, the computational code that was used: the two-equation Menters Shear Stress Transport (SST) $k-\omega$ model and the explicit algebraic stress model (EASM). A description of these is available below.

Menters SST $k-\omega$ model

The SST $k-\omega$ model was proposed by Menter in 1992 to improve the performance of the near-wall turbulence modeling of the commonly used two-equation $k-\epsilon$ model. The SST $k-\omega$ model uses the turbulent kinetic energy k, the turbulence frequency $\omega = \epsilon/k$ (dimension s^{-1}) and the Boussinesq assumption to compute the Reynolds stresses. The Boussinesq assumption is the presumed relation linking the Reynolds stress tensor to the velocity gradients and the turbulent viscosity. When a turbulence model uses the Boussinesq assumption, it then qualifies to be called a linear eddy viscosity model. This two-equation turbulence model uses one modeled transport equation for each of the two variable, k and ω. The ω equation is derived from the ϵ equation in the $k-\epsilon$ model by simply substituting the relation $\epsilon = k\omega$. Those equations are not displayed here in detail but it is insightful to understand the way those transport equations are built. For both equations, the structure is as follow [18]:

$$\begin{aligned} &\text{Rate of change of } k \text{ or } \omega \ + \ \text{Transport of } k \text{ or } \omega \ = \\ &\quad \text{Transport of } k \text{ or } \omega \text{ by turbulent diffusion} \\ &\quad + \text{ Rate of production of } k \text{ or } \omega \\ &\quad - \text{ Rate of dissipation of } k \text{ or } \omega \end{aligned} \tag{2.18}$$

The SST $k-\omega$ model blends the benefit of the Wilcoxs $k-\omega$ model at the near-wall and the performance at the freestream and shear layers of the $k-\epsilon$ model. This is why the Menters SST $k-\omega$ model is suitable for a wide range of CFD application [13]. Additionally, assessments of this turbulence model have suggested that it gives superior performance for adverse pressure gradient boundary layer [18]. An adverse pressure gradient leads to lower kinetic energy of the fluid and hence reduction of its velocity. If the pressure increase is large enough, the fluid direction can be reversed and that is what happens in flow separation, a phenomena that typically occurs at the transom of a boat such as the laser. Therefore, this turbulence model seems to be well suited for the current CFD application.

EASM model

To evaluate different turbulence models, the Explicit Algebraic Stress Model (EASM) is also assessed in the project to propose an alternative to linear eddy viscosity models (such as the SST $k-\omega$ model) that are based on the Boussinesq hypothesis. Often, linear eddy viscosity models fail at giving satisfactory prediction for complex three-dimensional flows due to the involvement of the Boussinesq assumption. Indeed, eddy viscosity models are unable to properly describe turbulence around curved surfaces because of the body force effects arising from the curvature. This leads to nonlinear stress-strain relations in turbulence modeling contradicting the Boussinesq assumption. [7]. These linear eddy viscosity models are however commonly used in the industry because of their high stability [18].

The EASM is a model that is derived from the original algebraic stress model (ASM) introduced by W. Rodi in 1976, which is not commonly used because of robustness issues and often-arising singular behavior [3]. The EAS Model addresses those issues by suggesting mainly two improvements. The first one concerns the treatment of the non-linear term due to the production-to-dissipation rate ratio that appears in the algebraic stress equation. The second one regards the number of tensor basis used to represent the explicit solution of those equations. Three-term tensor offers an exact solution to the two-dimensional algebraic stress equation but only gives an approximation to the three-dimensional problem. Gatski and Speziale [7] have come up with an exact solution for

three-dimensional flow involving ten-term tensor but this is too complex and requires too high computational power. Several group of researchers have worked to find an alternative to the ten-term tensor and most have found that using five terms yields to acceptable approximation of the solution to the algebraic stress equation [3]. EASM offers a solid answer to the original disposition to become independent of the Boussinesq assumption, however the model can become very complex and computationally demanding.

2.3 The volume of fluid method, VOF

The VOF is a multiphase flow method. This means it computes the interaction of several fluids or phases of a fluid present in the same domain. The purpose of implementing this method in yachting applications is to include the computation of the free water surface around the hull of the yacht.

In the VOF method the same Navier-Stokes euation as in single phase flows is solved. The difference is a phase indicating function γ [14]. The phase indicating function γ is also called color function or volume fraction. What it does is to display the measure of the mixture of phases in each cell. For example if $\gamma = 1$, the cell is completely occupied by phase one, and if $\gamma = 0.3$ there is 30 % of phase one and 70% of phase two present in the cell. For yachting applications the two fluids present are: water and air. As the air is included in this method, the spatial discretization has to extend above the waterline as well. This does of course increase the computational effort of the simulation, but it gains a physically more accurate representation of the waves, as will be explained later in this section.

The physical fluid properties used in the Navier-Stokes equation for a multiphase flow is a blend of the properties of the present fluids. In the case of yachting the present fluids are air and water. The computational properties are then blended in the following way :

$$\rho = \rho_w \gamma + \rho_a (1 - \gamma) \qquad \mu = \mu_w \gamma + \mu_a (1 - \gamma) \tag{2.19}$$

To track the motion of the interface a separate transport equation for the color function is used:

$$0 = \frac{\partial \gamma}{\partial t} + v_i \frac{\partial \gamma}{\partial x_i} \tag{2.20}$$

This method does however give rise to a numerical problem of the boundary between the phases being smeared over several cells. The smearing means that the water surface appears to be a gradual change in density between water and air. As the water surface is a discontinuity, a jump in density, the smearing is an unwanted phenomenon. This is a result of that the convective averaging is done across the water surface. The remedy for this is to implement, in the code, a way to detect when a boundary is present [8] and treat these areas separately. In the Shipflow software the smearing problem is dealt with by implementing a compressive discretization scheme, as suggested in [10].

To make the surface of the water visible the distribution of the color function is evaluated. Where $0 < \gamma < 1$ there is a mixture between the fluids and the free water surface is found. As mentioned however, the boundary between the phases may be smeared and therefore a specific value of γ is selected to display the surface.

The VOF method belongs to the class of surface capturing methods. This means that the interface between two fluids is computed somewhere inside the domain. The main difference from single phase, surface *tracking* methods, is that the dynamics of the air is also computed. In the single phase methods the water surface geometry makes the top boundary of the domain, and does therefore not take the air into account. The geometry of the top of the domain is then in every time step or iteration updated according to the kinematic and dynamic free surface conditions, and a new grid with new top geometry is generated for the next iteration [9]. The free surface conditions are automatically satisfied in the VOF method. Furthermore the surface capturing methods have

the advantage of being able to capture overturning waves, drops and complex surface features, if the resolution of the grid is fine enough.

The advantages of the VOF method in form of physical representation is considered to outweigh the disadvantages of computational cost and numerical instability and will therefore be used for all resistance computations in this thesis.

2.4 Verification

2.4.1 Overview

A CFD (computational fluid dynamics) simulation is used to give a detailed view of the fluid flow past a given geometry. The simulation is governed by equations of the flow properties. The equations are the mathematical way of expressing the conservation laws of physics (mass, momentum, energy). These equations are nonlinear and an iterative procedure is needed to obtain results. The results, in the Eulerian framework, are fields of the flow properties, for example velocity or pressure.

The flow field properties are then used to evaluate and quantify the sought result. In this investigation the hydrodynamic force acting to slow down the hull is the quantity of interest. To obtain the total resistance force the pressure and viscous forces at each cell on the hull is evaluated and then summated.

As the governing equations are implemented in a computer code the fields have to be discretized into smaller fluid particles, hereby referred to as a domain of cells, to which the equations are applied. The differential equations have to be linearized and schemes applied to estimate the derivatives. The size of the cells in the domain has impact on how well the flow is represented. In general the smaller the cells are, or the larger amount of cells that the domain contains, the better the flow field is represented [18]. The number of cells will influence to a high extent how computationally demanding the simulation will be.

The flow properties are stored in the center of each cell. The cells however interact by their adjoining boundaries, which means that the quantities have to be interpolated to the boundary from the centers. This is done an interpolation scheme implemented in the code. To define how well the interpolation scheme is performing in terms of accuracy, a Taylor expansion of a convective term (a derivative) is done [2]. When the low order terms are canceled the one left with lowest degree of dependency on the cell size, defines the order of accuracy of the scheme. The higher order terms in the Taylor series are neglected and the sum is truncated to only contain the one defining term. As the Taylor series extends to infinity the higher order terms have smaller and smaller effect on the error and as the cell size decreases they are considered to have small impact and are therefore, in this regard, neglected.

For example if a scheme has second order accuracy it means that the error will decrease to the square of the decrease in cell size. However the theoretical order of accuracy, or decrease in error, might not be observed when refining the grid. The reason for this can be that the refinement of the grid is not completely uniform. The wall distance for a turbulence model to be activated might not be scaled correctly or the aspect ratio of the cells might change. Another explanation for not obtaining the theoretical order of accuracy is that the truncated higher order terms, in the Taylor expansion, are in fact important to represent the behavior of the error decrease, for the particular case at hand.
The difference between the real flow case and the simulated one, in any given property, is here referred to as error. The error can then be subdivided into two categories: physical modeling errors and numerical modeling errors. The physical modeling errors originate from a faulty model of the physical phenomena at hand, for example use of inadequate equations. The numerical modeling errors comes from the procedure of solving these equations in the computer; rounding off numbers in the computer, incomplete convergence, insufficient spatial discretization or a diffusive discretization scheme [9].

To ensure that the CFD simulation is trustworthy a quantification of the expected error has to be made [12]. This section will thus explain how to quantify the spatial discretization error. The other numerical modeling errors are excluded from this part of the study, this is possible if the grid refinement factor r is above 1.1 [15]. The meaning of the grid refinement factor and how it is used will be explained later on. The study when the physical errors also are included are discussed in section: 2.5 Validation. However in the validation the numerical modeling and physical modeling errors cannot be distinguished.

2.4.2 Grid dependence study

The grid dependence study, also called grid convergence study, aims at observing how a chosen variable, S, changes with a change in the spatial discretization. The variable in this study will be the total resistance force of the dinghy. The resistance force will then be plotted as a function of the cell size h. To get the resistance force at the case where the cell size goes to 0, (the number of cells in the domain goes to infinity) the data points are curve fitted and then extrapolated towards 0. This is done by a certain method that originates from the Richardson extrapolation method, both will be explained in this chapter. This is done in order to show how the solution could have looked like if the flow was solved in a continuous domain. The result at zero cell size is in this thesis called S_0. Furthermore the grid dependence study can also provide a guide to which density of the grid that should be selected for a given uncertainty or an accepted error.

2.4.3 Richardson extrapolation

The purpose of this method is to find the interpolated value S_0, then the error of the simulations δ_{RE} can be found. The error is defined as the difference between S_0 and S_i, being the value at the selected cell size h_i. Obtaining several discrete solutions to the function $S(h_i)$, it can be assumed that the trend of the error will follow the following function:

$$\delta_{RE} = S_i - S_0 = \alpha h_i^{p_a} + higher\ order\ Taylor\ polynomials \tag{2.21}$$

The discrete solution will be a simulation at a certain cell size, or grade of refinement. Using the analytic order of accuracy p_a obtained from the leading order term of the Taylor series, the *classic* Richardson extrapolation can be performed. Two discrete solutions are then required to solve for the two unknowns S_0 and α.

$$S_i = -S_0 + \alpha h_i^{p_a} \tag{2.22}$$

As mentioned in the previous subsection the observed order of accuracy will differ from the analytic one to a certain extent. This can be because of dependence of the previously neglected higher order terms. To obtain a better more accurate estimation of the continuous solution for S_0 the *generalized* Richardson extrapolation method is used. In this method the observed order of

accuracy p_o is also solved for. Solving for the observed order of accuracy is done by considering the higher order Taylor polynomials and taking their effect into account in the power p_o, instead of including them in the equation [20]. As the obtained order of accuracy probably will not be the same as the analytic one there are now three unknowns. A minimum of three solutions are then required, which means that results from three grids has to be obtained. The formula for the generalized Richardson extrapolation is then:

$$S_i = S_0 + \alpha h_i^{p_o} \tag{2.23}$$

The three solutions forms a nonlinear system of equations that have an analytic solution[12]. Where r denotes the constant grid refinement factor $r = {}^{h_{i+1}}/_{h_i}$ and $\varepsilon_{ij} = S_i - S_j$.

$$p_o = \frac{\ln \frac{\varepsilon_{32}}{\varepsilon_{21}}}{\ln r} \tag{2.24}$$

$$\alpha = \frac{\varepsilon_{21}}{r^{p_o} - 1} \tag{2.25}$$

$$S_0 = S_1 - \frac{\varepsilon_{21}}{r^{p_o} - 1} \tag{2.26}$$

Application of Richardsons method

The Richardson interpolation shall be used when the solutions are in the asymptotic range of convergence. This means that the cell size has to be sufficiently small for the higher order terms to be insignificant. This criterion can be quantified in two ways [11].

Having the three solutions in the asymptotic range means that influence of the higher order terms can be disregarded and in turn the uncertainty will be well predicted. The limitation of this method is however that the grids have to be very fine in order to achieve the asymptotic range [4]. The fact that this requires large computational effort made it not suitable for this thesis. The method for dealing with the scatter of grids considered too coarse for the explained method is proposed in [4]. The three coefficients are then found by least square root curve fitting method, LSR. The three coefficients to equation (2.23) are then found by minimizing the following expression:

$$f(S_0, \alpha, p_o) = \sqrt{\sum_{i=1}^{ng} \left(S_i - \left(S_0 + \alpha h_i^{p_o}\right)\right)^2} \tag{2.27}$$

As a comparison the coefficients for equation (2.22), using the analytic order of accuracy p_a, can be found in the same way, by minimizing:

$$f(S_0, \alpha) = \sqrt{\sum_{i=1}^{ng} \left(S_i - \left(S_0 + \alpha h_i^{p_a}\right)\right)^2} \tag{2.28}$$

Using this method more than three grids are required in order to account for the scatter. In this thesis 6 grids will be used.

2.4.4 Uncertainty

As mentioned the Navier-Stokes equations for the flow around the hull is not directly solved, there are numerical models applied to the simulation in order to limit the required computational effort. In the case of doing so not only the error based on the difference to the test results is of interest, the uncertainty of the simulation itself is also of significance [21]. The uncertainty is the interval in which the exact solution is expected to be found.

There are three different methods of obtaining the uncertainty U_{sn}: the grid convergence index also called GCI, the factor of safety method also called FS and the least square root curve fitting method, LSR. The one chosen for this thesis is the LSR. This method of quantifying the uncertainty is based on the error of the Richardson extrapolated curve, fitted to the result data of the different grids in the study, described in section 2.4.3.

The purpose of this method is to try and include the exact solution within the error band with a 95 % confidence [5]. The method for doing this is made and adjusted to fit test result presented at the workshop of [5] and in the paper [4]; this is an empirical method. The way to compute the uncertainty with the LSR method is governed by the observed order of accuracy p_o, in the following way:

1. If $p_o > 0$:

$$0.95 \leq p_o \leq 2.05 : U_{sn} = 1.25\delta_{RE} + U_{sd} \tag{2.29}$$

$$p_o \leq 0.95 : U_{sn} = min\left(1.25\delta_{RE} + U_{sd},\ 3\delta_{RE}^{12} + U_{sd}^{12}\right) \tag{2.30}$$

$$p_o \geq 2.05 : U_{sn} = max\left(1.25\delta_{RE} + U_{sd},\ 3\delta_{RE}^{02} + U_{sd}^{02}\right) \tag{2.31}$$

2. If $p_o \leq 0$ and $\sum_{i=2}^{n_g-1} n_i \geq INT\left(n_g/3\right)$, where $n_i = 1$ if $\left(S_{i+1} - S_i\right)\left(S_i - S_{i-1}\right) < 0$:

$$U_{sn} = 3\delta_{\Delta M} \tag{2.32}$$

3. Else :

$$U_{sn} = min\left(3\delta_{\Delta_M},\ 3\delta_{RE}^{12} + U_{sd}^{12}\right) \tag{2.33}$$

Where:

- the δ_{RE}^{02} and the δ_{RE}^{12} are obtained from curve fitting the following functions in the same manner as described above in section 2.4.3

$$\delta_{RE}^{02} = S_i - S_0 = \alpha_{02} h_i^2 \tag{2.34}$$

$$\delta_{RE}^{12} = S_i - S_0 = \alpha_{11} h_i + \alpha_{12} h_i^2 \tag{2.35}$$

- the δ_{Δ_M}:

$$\delta_{\Delta_M} = \frac{\Delta_M}{\left(h_{n_g}/h_1\right) - 1} \tag{2.36}$$

  Where the Δ_M is the maximum data range, $max\left(|S_i - S_j|\right)$.

- the U_{sd}, U_{sd}^{02} and U_{sd}^{12} are the standard deviations of the curve fitted functions: 2.23, 2.34 and 2.35. For example for equation 2.35, the standard deviation is found by minimizing the following expression:

$$U_{sd} = \sqrt{\frac{\sum_{i=1}^{ng}\left[S_i - \left(S_0 + \alpha_{11}h_i + \alpha_{12}h_i^2\right)\right]^2}{n_g - 3}} \tag{2.37}$$

2.5 Validation

The investigation of the effect of heel and trim on the dinghy will be preceded by a validation and verification study of one case from the towing tank test runs. It will be a bare hull case, without appendages or leeway. This case will have a zero degrees angle of heel which means that the geometry will be symmetric along the center line if the dinghy. This fact will be used in the simulations to half the number of computational cells by running a symmetric simulation. A H-O-grid will be used for this simulations.

2.5.1 Formal procedure

The goal of the validation procedure is to see if the combination of all the errors in the study, E, adds up to be smaller than the uncertainty of the validation procedure, U_V. If this is the case the simulation can be regarded as validated to the level of uncertainty U_V [16]. The procedure of how to obtain these quantities will hereby be explained.

The result on which the validation study is based is the total resistance. The true value of the total resistance of the dinghy, T, is said to be the result for the chosen method minus its estimated error. The resulting total resistance obtained by the towing tank test, the data, is in the validation study called D. Similarly for the simulation: S. The corresponding error is called δ_i. This is stated in the following way:

$$T = D - \delta_D \qquad T = S - \delta_S \tag{2.38}$$

The difference between D and S is called the comparison error E, on which the validation is based.

$$E = D - S = \delta_D - \delta_S \tag{2.39}$$

The error of the simulation δ_S is then decomposed into specific contributing factors $\delta_S = \delta_{model} + \delta_{numericals} + \delta_{input}$ [17]. The uncertainty of E, U_E, is expressed as the absolute value of the data and simulation uncertainties: $U_E = \sqrt{U_D^2 + U_S^2}$, and decomposed in the same manner.

$$U_E = +\sqrt{U_D^2 + U_{model}^2 + U_{sn}^2 + U_{input}^2} \tag{2.40}$$

This decomposition reveals the uncertainty of the modeling error, which is a component that is not known. The modeling error contains possible errors connected to any assumptions made setting up the model. As this quantity is unknown so is its uncertainty U_E and consequently the calculation of the validation uncertainty U_V has to be done without this contribution. The U_V is therefore said to be the absolute value of the known uncertainties. The subscript sn is referring to numericals, this notation corresponds to the one in the grid dependence study (see section **??**). This quantity did in turn contain contributions from both the grid and an incomplete iteration procedure. For This discussion see subsection 2.4.4. The uncertainty of input parameters can be of importance if the simulations are based on previous calculations or uses boundary conditions are estimated.

The uncertainty in the validation procedure is expressed in the following way.

$$U_V = \sqrt{U_E - U_{model}} = \sqrt{U_D^2 + U_{sn}^2 + U_{input}^2} \tag{2.41}$$

Roache (1998) decomposes the error of test data acquisition into two parts, bias error and precision error. The bias error is the part that can be reduced by calibrating the measuring device. The precision error is the interval into which data from identical tests will fall. In other words the precision error is the uncertainty of the test.

2.5.2 Numerical parameters

In this section, the following parameters configuring the validation case are described: the spatial discretization, the Froude number and the Reynolds number.

The grid has great influence of the results of any CFD simulation. The reason for this is that a partial differential equation is defined for a continuous field. As a computer cannot treat these kinds of equations, if no analytic solution exist, the partial differential equation in question has to be linearized on small pieces of the domain, which together makes the grid. Therefore if the grid is of poor quality the results of the simulation will also be poor. What is regarded as poor is dependent on the physics of each individual case or type of case, and the size of the turbulent scales that are to be resolved. The Shipflow software generates its own spatial discretizations. The types used in this thesis were a H-O-grid and a H-O-grid overlapped by an H-H-grid. The method of overlapping grids was used to be able to accurately specify the heel and trim angle of the dinghy. The grid settings are specified manually. The settings include the overall size of the domain, size of subdivisions in longitudinal and girth-wise direction and the cell density in the three spatial directions. A grid convergence study will be performed for each of the three validation cases, see section 2.4.

The velocity of the dinghy used for the validation study was set to 4 knots, or 2.06 m/s. The velocity is normalized by the length between perpendiculars, L_{pp}, according to function (2.42). The Froude number of the dinghy at 4 knots is then $Fr = 0.3393$,

$$Fr = \frac{v}{\sqrt{gL_{pp}}} \tag{2.42}$$

The motivation for the selected velocity is that it will result in that the transom of the dinghy is cleared of recirculating water. This was known from looking at the results from the towing tank test runs. A dry transom is desired to make the simulations more numerically stable. The trim angle and heel angle will be fixed for the grid generation, to match the angles obtained at speed during the runs in the towing tank. These angles are not estimated in the simulation because the test setup introduced an unnatural trimming moment, discussed in section 1.6.3.

The turbulence model is another setting that will influence the result of the simulation. To display the level of turbulence or the inverse of the size of the smallest turbulent scales, the Reynolds number Re is computed using the following formula:

$$Re = \frac{vL_{pp}\rho}{\mu} = \frac{vL_{pp}}{\nu} \tag{2.43}$$

The length of the dinghy and the selected velocity makes the flow highly turbulent. For the 4 kts case $Re = 7488268$. This means that the smallest scales are very small indeed and in order to resolve them the grid have to be very fine. As mentioned before the equations have to be time averaged to make simulations on a coarser grid possible, this operation however introduces unknown quantities that have to be modeled: the turbulent stresses. As the different models does this with different rates of accuracy for different cases or in different parts of the domain they have to be selected carefully. The selected code, Shipflow, provides the choice of two different turbulence models: $k-\omega-SST$ and $EASM$. For a more thorough discussion on turbulence models see section 2.2 .

3

Numerical Methods and CFD Solver Shipflow

Computational Fluid Dynamics (CFD) codes are developed to analyze, predict and solve fluid flow, heat transfer and associated phenomena. In order to input parameters and view the results, a user interface is necessary. That is why such codes always contain three main components: a pre-processor, a solver and a post-processor [18].

The pre-processor's role is to let the CFD user input parameters that define the problem. This involves setting the domain size and geometries involved, the grid generation, the flow velocity, fluid parameters and other instructions for the solver.

The solver part of a CFD package is the code that can solve the partial differential equations in the computational domain by discretizing the differential equations in space and time. In this discretization segment, the differential equations are approximated by a system of algebraic equations for the variables (such as velocity or pressure values) at the discrete points over the domain that were defined in the grid generation portion of the pre-processor [20].

Finally the post-processor's function is to view and analyze the results of the solver. It usually comprises a graphical user interface where the grid and the domain can be displayed. It also includes functionalities to plot various significant data.

3.1 CFD solver Shipflow

The commercial CFD package that was used in this thesis project is called Shipflow and is developed at Flowtech International AB in Gothenburg, Sweden. This CFD solver is tailored to help naval architects investigate fluid flow and resistance forces around the ship's hull design. Without exception, this package also contains the three main elements cited above.

There are several different methods that can be applied in the Shipflow software that are based on different assumption and therefore result in different amount of information about the flow. There is an inviscid panel method, a boundary layer method for estimating viscous resistance and a RANS solver for both single and multiphase flow. Shipflow can also use a zonal approach where the computational domain is divided into three zones where both the panel, boundary layer and

RANS solver is used together. In this approach, the boundary layer zone that is located closed to hull at the forward part of the hull is handled by the boundary layer method. The wave resistance is predicted by the panel method and only the stern section of the ship is resolved with of the RANS method. The RANS zone is located behind the hull, in the wake, where the boundary layer approximation does no longer apply. The reason for dividing the domain in such way is to decrease the size of the volume for the computationally demanding RANS solver.

In this thesis however, a global approach is preferred rather than using the zonal approach described above. Discretizing the whole domain is as mentioned more costly but will return more accurate results. Discretizing the whole domain is also a requirement for using the volume of fluid (VOF) method, which is the multiphase flow method. This method is described further in section 2.3. It is deemed suitable for this application because a higher accuracy in computing the free surface is expected, despite possible minor numerical instability and heftier computational requirements.

The two main solver modules of Shipflow that are used in the global approach to resolve the flow and the resistance forces are: Xgrid and Xchap. Many other modules exist in Shipflow, for example used in the zonal approach, but are not described in this report. Xgrid is the module that lets the user input parameters to arrange the computational domain around the hull of the ship in details. It is possible to define the grid around the hull in all three dimensions. Various zones around the geometry and the domain can be setup separately allowing choosing for appropriate grid density according to areas of interest. The Xchap module utilizes the grid configuration from Xgrid to resolve the RANS equations using two possible turbulence models: $k-\omega$ SST and EASM. Selecting an appropriate turbulence model is crucial when resistance forces predictions are needed, giving rise to a special investigation for which the results are presented in 4.1.4. The Xchap solver can be used both in a zonal or global approach. Xchap computes quantities such as the velocity field, the pressure, the turbulent kinetic energy, local skin friction coefficient and most important to this investigation the friction, pressure and total resistance coefficients.

3.2 Grid definition

This section provides a description of the grid configuration in the computational domains used for the simulations, and which boundary conditions that was applied. Three different structured grids are in use to cover every part of the domain: H-O-grid, H-H-grid and O-O-grid. The grid type refers to the shape of the grid domain. The first two grid layouts are displayed in figures 3.2a and 3.2b respectively. The dome shaped O-O-grid is used around the appendages and can be observed in figure 3.3b.

3.2.1 Description of the Computational Domain

Xgrid generates the structured H-O-grid that is defining the domain around the hull. This grid layout is desirable because it will generate cells that are roughly aligned with the direction of the flow and are fitted to the geometry. Generally stretch functions are applied to the distribution of the cells in order to increase cell density in the vicinity of the hull. The near-wall cells have to be very thin for the velocity profile in the boundary layer to be represented with a good resolution. It is important to have a good representation of the velocity profile in this area as the gradient of which is defining the amount of viscous resistance. The near-wall cells distribution can be observed in the figure 3.1

One can note that no wall function is used to approximate the behavior of the flow in the near-wall region.

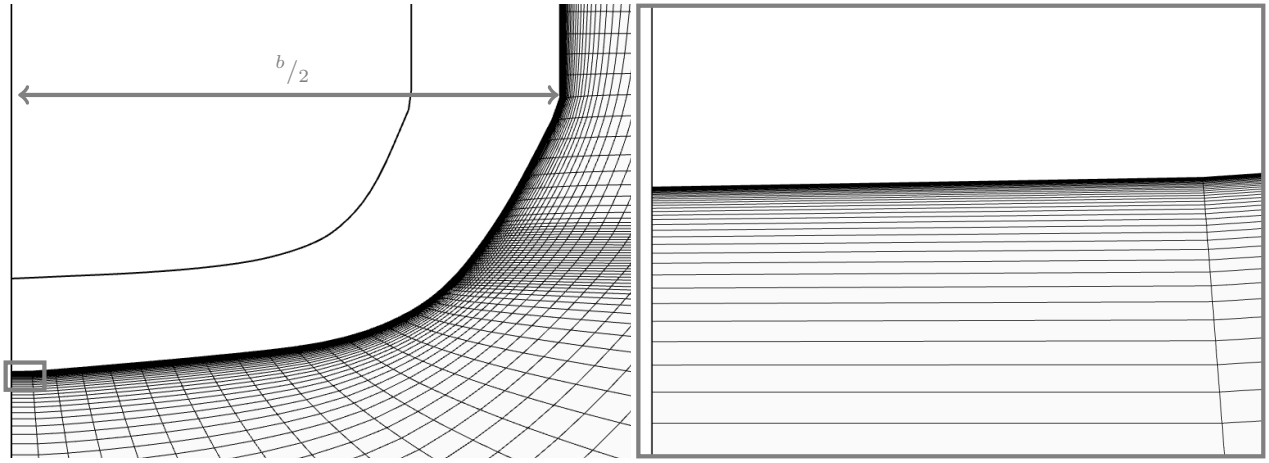

(a) View from stem (b) Closeup of near wall cells

Figure 3.1: Display of the cell density near the walled boundary of the hull. $y_1^+ \approx 1$.

The H-O-grid layout is used alone, as displayed in figure 3.2a, only in the verification and validation phase because the hull is then oriented straight against the flow (no leeway) and is upright (no heel angle) which means that the case is symmetric. In symmetric cases, the flow is only computed on one side of the hull and assumed to be exactly symmetric for the other side.

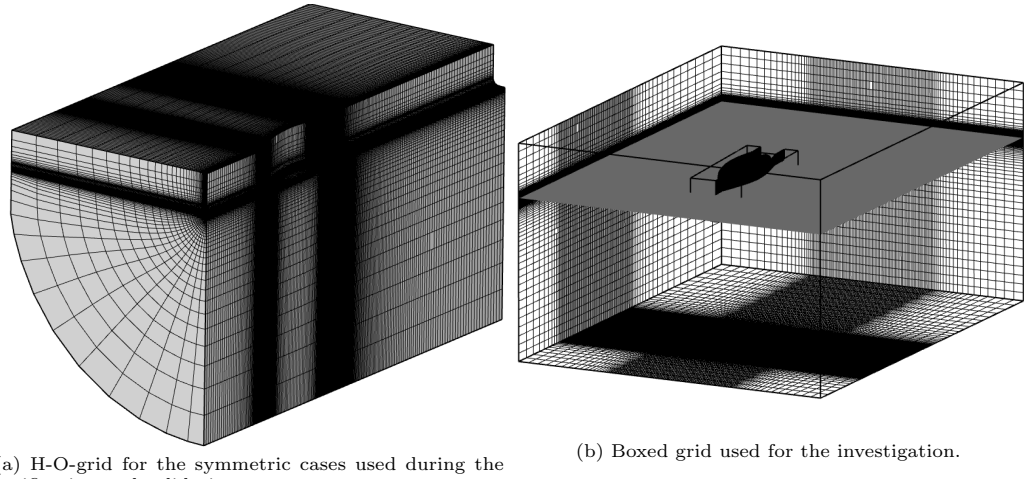

(a) H-O-grid for the symmetric cases used during the verification and validation.

(b) Boxed grid used for the investigation.

Figure 3.2: Overview of grid types.

The H-H-grid, also called box, is used as the main structure for the simulations of the heel and trim variation investigations. This grid layout is shown in figure 3.2b. The geometrical representation of the dinghy's hull and the appendages was then added to the domain as overlapping component grids. When the component grids were added they were also given the selected angles of heel and trim corresponding to the ones obtained at speed during the towing tank tests.
Seen in figure 3.3 is a close-up on the component grids for the box grid cases. The grid that

is defining the hull shape is still a H-O-grid identical to the one used for the symmetric cases, but with a more narrow fit to the hull. The advantage of keeping the H-O-grid around the hull is double. Firstly because of the near-wall cell definition as explained earlier and secondly because this configuration allows for a simple rotation of the whole H-O-grid around the x and z-axis to mimic the heel and leeway angles for which the test is setup. This is illustrated in the figure 3.3a.

The component grids defining the appendages are O-O-grids as shown in the figure 3.3b. Here again, the O-O-grids become an overlapping component grid of the H-H-domain and is then rotated along with the hull's H-O-grid in the heel variation investigation.

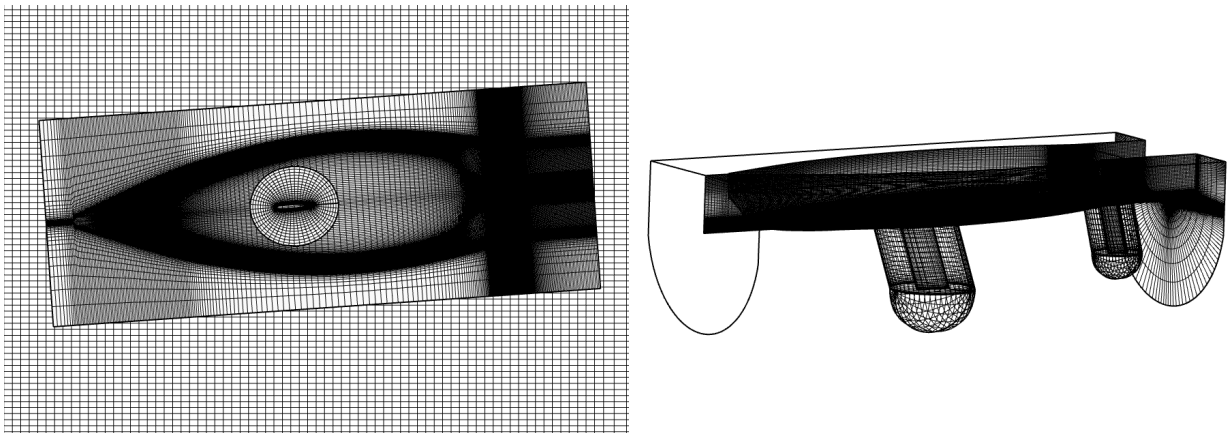

(a) Topview (b) Isometric view

Figure 3.3: Display of the subgrids used for the investigation cases with appendages and leeway.

3.2.2 Appendages modeling

The appendages can be modeled in two ways in Shipflow; either the geometries of the appendages are imported like the geometry of the hull or they can be created from a selected wing profile within the software. The chosen way was to create the appendages in the software. To do this the particular wing profile of the rudder and centerboard had to be determined and the overall dimensions and positions measured. The appendages are then added into the domain as separate component grid with a walled boundary defining the geometry.

3.2.3 Boundary Conditions

The boundary conditions for the domain are displayed in the following figure. The slip boundary condition is in practice the same as symmetric, which is why the symmetry boundary is also marked slip. The space above and behind the dinghy is also discretized in two separate grids which are removed from the figure for better visibility.

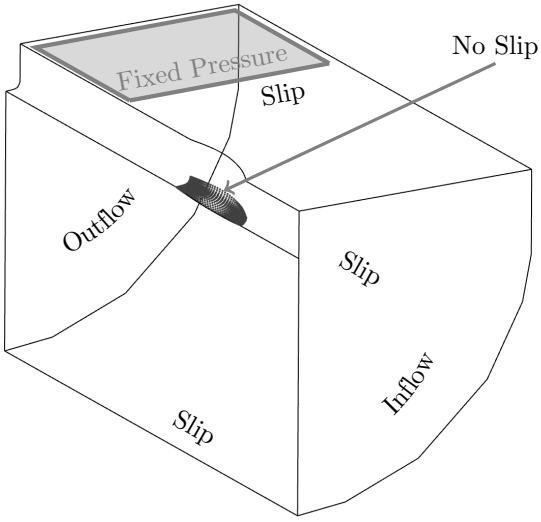

Figure 3.4: Boundary conditions for the symmetric domain. The same boundary definition is valid for the boxed grid.

3.3 Data comparison

As the towing tank test were performed using a force measuring device that gave readouts in Newton and the CFD software gave results in terms of the dimensionless drag coefficient, the results from the simulations had to be converted to absolute forces. This was done by using the definition of drag coefficient [19]:

$$F = C_D \frac{1}{2} \rho U^2 S \tag{3.1}$$

Where S is the wetted surface area of the hull and U is the boat speed.

4

Systematic Variation of Numerical Parameters

4.1 Parameter studies

The work presented in this chapter was initially done to improve the result of the validation. The first results of the grid dependency study revealed that the best simulations predicted a resistance of around 7% less than the towing tank tests. This result was judged unsatisfactory leading to a systematic variation of the numerical parameters presented in this section in order to evaluate their effects on the results. The improvements that resulted from the systematic investigations were used to produce the verification plot presented in the last section of this chapter.

From the first simulations, it could be observed graphically that the transom was not cleared of water, as it should be according to the towing tank test results. This led to a first investigation to see if the grid density in this area of the domain could have an effect on this wave. In order to figure out how to improve the result of the validation, the parameters of fluid density ratio, height of domain and convergence criteria also was selected for systematic investigation. Finally an investigation aimed at selecting the best turbulence model is also included in this section. The results of these investigations will hereby be presented for future reference.

4.1.1 Fluid density ratio

This investigation was considered valuable for this thesis as the density ratio that was set as default by the software was not physically accurate. This has previously been mentioned in section 1.7. The motivation for using a nonphysical value for the density ratio is that the simulations become more numerically stable for values closer to one, which means two fluids of the same properties. The result of this investigation can be seen in the following figure.

Concluded from the figure 4.1 is that the trend is diverging as the density ratio decreases and goes towards a value of the physical density ratio $r_\rho = 0.0013$. No results from values below 0.0013 are reported because these simulations did not converge.

The difference of 0.90 % decrease from 0.0013 to 0.01 is not considered to be insignificant. However as the results in the region of low density ratio is diverging rapidly these results is not trustworthy

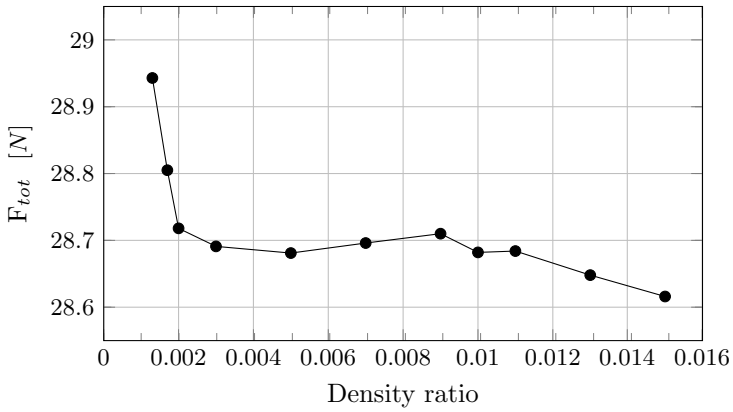

Figure 4.1: Result of density ratio investigation. The default value in Shipflow was set to 0.01. The percental difference from 0.0013 to 0.01 is 0.90 % decrease.

and this quantification shall be viewed with caution.

The conclusions of this investigation was that the results seem to reach a plateau at $r_\rho = 0.005$ and the fact that a higher density ratio really did make the simulation more stable, and only a small increase in resistance was obtained, it was decided to continue the thesis work with the density ratio set to 0.01.

4.1.2 Convergence criteria

This investigation was done in order to see how the result in terms of total resistance was affected by the convergence criteria.

This investigation was performed because of that the simulations were finished at different levels of convergence. This was the result of manually finishing the simulations when they showed a convincing level of convergence. The default convergence criteria is at $< 1\%$ of standard deviation in the pressure component of the resistance, in the longitudinal direction. (The residuals can also be used to display convergence in the Shipflow software.)

For this investigation 5 identical simulations for a reference case were started. The simulations were then automatically finished when the selected convergence criterion was reached. Concluded from this investigation was that below the default criteria there were no significant change in resistance. This meant that the preferred manual way of finishing simulation was acceptable as long as the default convergence criterion was exceeded. The results of the investigation are displayed in the following figure:

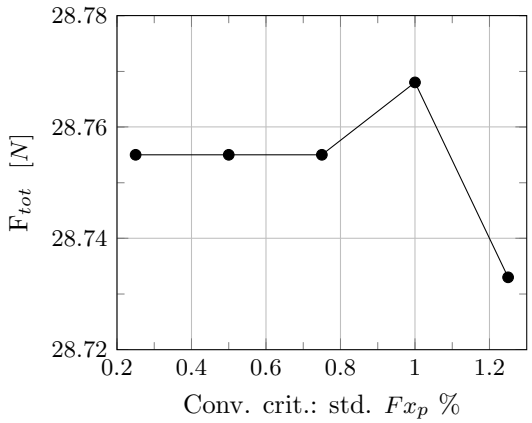

Figure 4.2: Result of convergence criteria investigation. The default value in Shipflow was set to 1%. The difference between 1 and 0.25 is 0.05 % decrease.

4.1.3 Domain height

This investigation was started in order to see the effect of the height of the domain, on the free water surface geometry in the transom area, again to see if the transom wave could be eliminated. The effect this could have on the total resistance was also of course of interest. The height of the domain here refers to the height of the volume above the water surface, occupied by air.

The top boundary of the domain, in the downstream and middle part has a fixed pressure. This Derichlet boundary condition is implemented on this area to act as a reference for the pressure during the simulation.

The number of cells in the z direction was kept constant when the domain height was changed. The results of this investigation can be seen in the following figure:

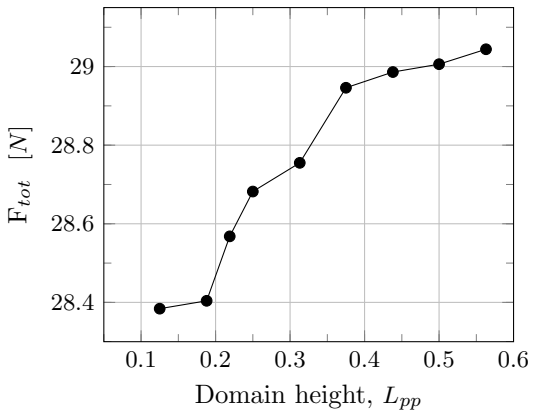

Figure 4.3: Result of domain height investigation, domain height refers to the height above the static water surface. Default value in Shipflow was set to 0.5.

Concluded from the figure is that the resulting force increases rapidly until 0.375 L_{pp}. The result

from the investigation shows a decrease by 2.27% from 0.563 to 0.125, with a plateau starting 0.375 L_{pp}. Domain heights over 0.563 L_{pp} gave a diverging trend in resistance.

Concluded from this investigation was that the domain height shall be set to 0.5 L_{pp}, or in this particular case 2 meters, in order to still be in the region of numerical stability but also give a resistance as close to the towing tank test result as possible.

4.1.4 Turbulence Models

The software Shipflow implements two turbulence models: $k\omega - SST$ and EASM. For a discussion on these see section 2.2. As the different turbulence models give good results for different types of flows both of these was tested on the validation case. The results are presented in the following table.

$\#\ cells,\ M$	$Turb.\ mod.$	$A_w,\ [m^2]$	$F_{tot}\ [N]$	$Difference$
4.9	$k\omega - SST$	3.155	29.00	-6.8%
4.9	EASM	3.168	27.05	-13.0%
5.4	$k\omega - SST$	3.155	29.04	-6.6%
5.4	EASM	3.170	26.64	-14.3%
6.4	$k\omega - SST$	3.154	29.10	-6.44%
6.4	EASM	3.173	26.57	-14.6%

Table 4.1: Result of the turbulence model investigation for three different grids.

Concluded from this investigation is that the $k\omega - SST$ model is the superior one for this case. The EASM did not only predict a too low total resistance, it also took a lot longer to converge. The medium dense grid with the EASM converged with an oscillating trend and a mean value over 2000 iteration had to be selected. This interval represented roughly two periods of the oscillating behavior.

The $k\omega - SST$ was then used for the forthcoming simulations.

4.1.5 Cell Density in the Transom Region

This investigation also originated in having water creeping up on the vertical transom of the dinghy. The cause of this water was thought to be an insufficient resolution of the grid at the corner where the transom meets the bottom of the hull. Therefore this investigation of local grid refinement was started. The grid type used was structured which means that the grid refinement cannot be completely concentrated to this region alone. A refinement does therefore result in a large increase of cells in the domain. Another consequence of refining the grid locally in the transom area is the grid density at midships. Stretching functions are used in the meshing tool, Xgrid, which makes the very fine cells gradually grow larger with a certain factor. This makes the cells at midships rather large as a limited amount of cells are used to cover the length between perpendiculars. This could

have been avoided by adding more cells in this area, but as the transom was the area of interest in this investigation this was not done. The longitudinal direction was selected for refinement. The results of this investigation can be seen in the following table.

$Density,\ L_{pp}{}^{-1}$	$\#\ cells,\ M$	$F_{tot},\ [N]$	$Difference$
600	4.7	28.84	-7.14%
3'600	5.9	29.08	-6.50%
7'500	8.9	29.09	-6.46%
30'000	8.9	29.03	-6.65%

Table 4.2: Result of the transom grid refinement investigation. The cell density is in the lonitudinal direction, in the region aft of the transom. (To save computational effort the region of refinement is concentrated in the last case, which is why the cell count is still 8.9 million)

The conclusion of the grid refinement was that the transom water *could be reduced* by refining the transom grid, but it could not be totally cleared. However the sought gain in resistance was almost negligible and the cost for resolving the flow was significantly increased. This concluded that the transom grid was not the major cause of the too low predicted total resistance.

Discussion

Some of the cases run during the main investigation of the thesis converged to an oscillating behavior which can be due to the fact that the flow is not steady state after all. If the flow is unsteady in this region it can also result in that the steady state simulation gives this transom water as a result. To test if the flow is unsteady a transient simulation has to be done but as the Shipflow software did not have this option this was not investigated in this thesis.

Another way of obtaining an unsteady flow in the simulation is if the waves are not small enough when they are leaving the domain. The remedy for this will then be to increase the overall size of the domain in order for the waves to naturally dampen before reaching the boundaries. This was not systematically investigated due to lack of time, but can serve as a suggestion for future investigations.

4.2 Results of the verification

As mentioned in previous chapters several different grid setups were tested during the first part of the thesis. This was done in order to see if the spatial discretization could be the major contributing factor to the low prediction of total resistance in the bare hull simulations. The method for this was to change the cell density in different areas of the domain and then evaluate the effect in terms of the total resistance. Doing this did in turn result in the generation of six new grids with constant refinement ratio $r = \sqrt[4]{2}$, to get sufficient information for the grid dependence study.

As the results in terms of resistance were not significantly improved the study of systematic variation of numerical parameters was started. This section will show the results of the simulations

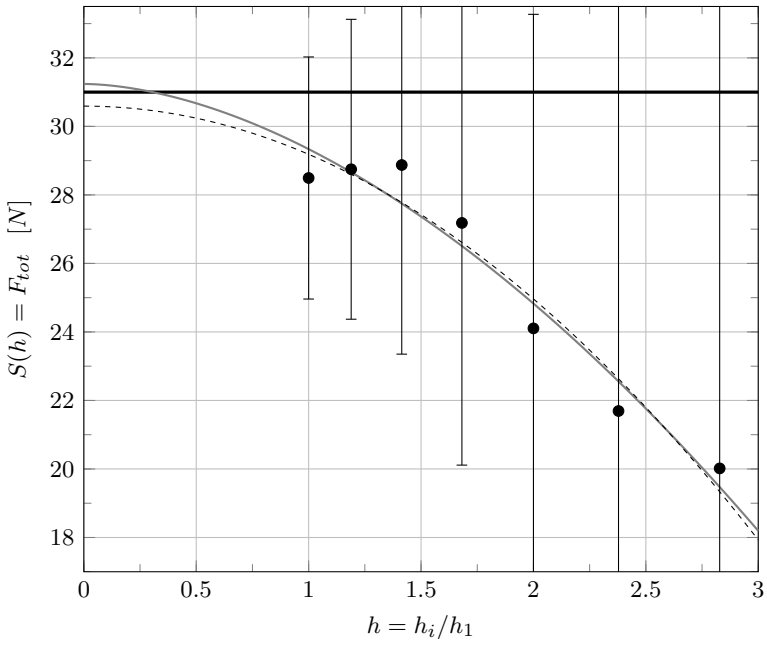

(a) Grid Convergence plot. *Even keel 4 kts.* Test data = 31.1 N; S_{0a}=30.59; S_{0o}=31.24; p_a=2; p_o=1.75. Where subscript a and o means analytic and obtained respectively. Grids are numbered staring from the left.
——— = Towing tank test; ——— = Obtained order of accuracy; - - - - - = Analytic order of accuracy

Grid	F_{tot} [N]	$\delta_{RE}/_{S_{0o}}$	*M cells*
0	28.49	8.8%	12.1
1	28.75	8.0%	7.2
2	28.87	7.6%	4.3
3	27.18	13.0%	2.6
4	24.10	22.8%	1.6
5	21.69	30.6%	1.0
6	20.02	35.9%	0.6

(b) Points data.

Figure 4.4: Results of the grid dependency study.

after the best settings from all the tested parameters were applied, and the grid dependence study rerun. Chosen in the beginning of the thesis was that the grid dependence study it should include 6 grids. This is the number that would usually be enough to get rid of the scatter that is present, explained in section 2.4.3.

Concluded from the plot is that there still is a large degree of grid dependency. This called for one further grid refinement, which is also displayed in the figure as *grid 0*. The seventh grid did not show any improvement in terms of total resistance but that can be due to the inevitable scatter. There are two sources for the scatter: the fact that the higher order terms are important to explain the behavior of the accuracy or that the grid refinement is not exactly systematic. The latter is always to some extent the cause, as aspect ratio or limits for activation of damping or such, might not be kept the same. Another reason for the lack of improvement in the finest grid could be that the change is too small to be noticeable in comparison to the next finest one.

Evident of this grid dependence study is that there is a strong grid dependency. This means that a substantial increase in grid definition should be able to eliminate the $\sim 7\%$ error. The problem associated with a further increase is the lack of memory on the machines, used for running the simulation during this thesis. The limit for the available 24GB seemed to be around 14.5 million cells. The next refinement of $r = \sqrt[4]{2}$ would result in ~ 20.3 million cells, but a higher refinement factor is probably needed as mentioned in the previous paragraph.

The conclusion of the grid dependence study in terms of which grid setup that shall be used for the investigation is the one from grid 2. Deciding which grid results in a reasonable error is weighted

against the computation time. As the grid 2 gives the best results and also had a reasonable computation time it was selected.

The grid dependency for an appendage and leeway case was not done as the grid settings for the boxed grid, required to include leeway, was not successfully changed. This was due to lack of knowledge in the meshing tool, which lead to an inability to arbitrarily refine the grid.

Further investigation of the grid dependency study

Doing this grid dependence study revealed that the selection of the finest grid had great influence on the outcome. As these different grid dependence studies showed in table 4.3, including different combinations of the provided grids, were evaluated it was also evident that including one more refinement could change the resulting parameters p_o and S_0 considerably. As one further refinement was done there was enough information for the study to include seven grids and because the LSR method does not have an upper limit of number of included grids, this was possible. The cases of fewer grids are included to display the negative effect of not having enough information when using this method.

$\#ofgrids$	$Grids$	p_o	S_0	$Difference$
6	1–6	1.04	36.21	16.6%
6	0–5	3.27	29.62	-4.64%
7	0–6	1.75	31.32	0.84%
5	0–4	7.10	28.89	-6.99%
4	0–3	21.10	28.69	-7.63%

Table 4.3: Result of the grid dependency investigation. The seventh grid refinement is called grid 0 as it was added to the study. Grid number 6 is the coarsest.

The extrapolation curve and the results of the study including all seven grids can be seen in figure 4.4a, the error bars represent the uncertainty of the simulations.

The cases of six grids show that a considerable span in the resulting coefficients can be obtained by defining the finest grid in a too coarse manner. This is the consequence of not having solutions in the asymptotic range. The scatter is therefore in this case considerably influencing the result. The conclusion was then that the choice of the finest grid in the study needed to be made with extra care in order for the LSR method to give reasonable values for the coefficients. Also concluded was that the more information that is obtained the better the outcome of the grid dependence study will be.

5

Validation Results and Discussion

The results from the validation study will hereby be presented, and the outcome discussed.

The main investigation of the thesis was to see if the minima in resistance could be predicted at the same angles of heel and trim, using the following methods: bare hull towing tank tests, bare hull simulations and simulations with appendages and leeway. If this is the case the more time consuming unsymmetrical simulations, needed for handling the leeway, can be rejected for future investigations of this kind. The leeway simulations with the appendages that is rudder and centerboard, are interesting because they represent the real sailing conditions in the most accurate way possible in a steady state setup, without oncoming waves.

The overall goal of the sports project is to help the sailors to improve their technique by using scientific measures in finding the optimum attitude to sail the dinghy. This will then include more effects than only hydrodynamic resistance, but this is what this thesis is limited to. Furthermore the angle of heel and trim for which the minimum of resistance is obtained, for a certain velocity, might be a combination heel and trim. A scenario like that was not included in the test matrix from the towing tank. What this means is that, only testing the cases of heel variation for zero trim and the trim variation for zero heel, can only predict a local minima in resistance. Another *combination* of angles of heel and trim, than found in these set of towing tank tests, might then give the global minima point.

As the tests were done for heel and trim variations separately it will also be presented separately in the following sections. However the full series of simulations of heel and trim variation was not completed. This was thought to be due to; lack of knowledge in the software, that it is still a young application of the VOF method and that it is usually handles ships of very different kind. The results of the simulations that are finished are shown in the following sections of this chapter.

5.1 Heel Variation

The results of the systematic heel variations are presented in the following figure. The bare hull simulations that are finished, and shall be validated against the towing tank test data, are still predicting very low resistance. This is despite the systematic variations of numerical parameters performed before.

Concluded from the available results from the four knots heel variation for the bare hull cases,

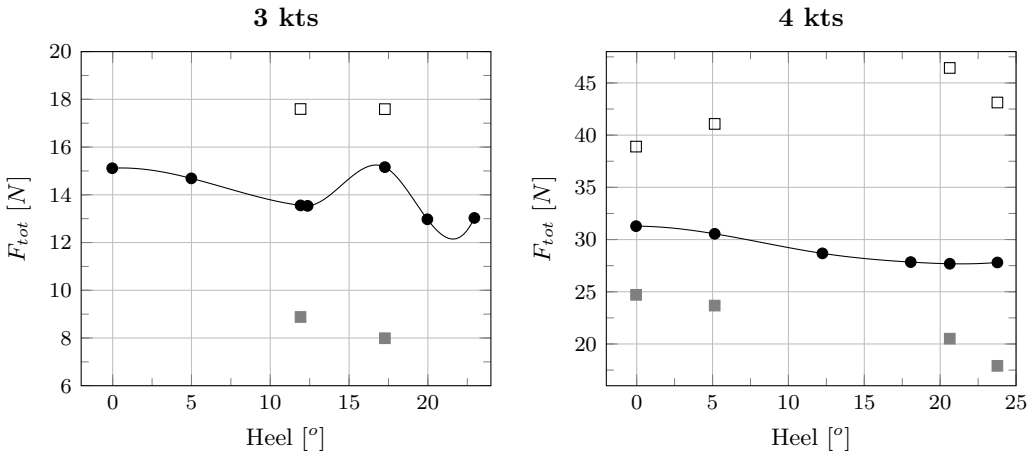

Figure 5.1: Result of heel variation. ● = Test data; ■ = Bare hull simulations; □ = Appendage and leeway simulations.

is that the error is larger than the error obtained in the verification study. The best grid density was then found to be one containing 4.3 million cells and the settings for this grid would now be used for all the simulations during the investigation. The exact grid settings could however not be used as the grid layout will be changed. The grid layout used in the verification study was H-O-grids, explained in section 3.2.1. For the investigations part however the boxed and overlapping grid was used. The reason for this was that the simulations including leeway could not be done in the H-O-grid. The bare hull simulations were also computed using the boxed grid during the investigations to eliminate the effect of different grid types on a comparison.

The setup of the boxed grid with the selected settings was however not done successfully. The reason for this was lack of knowledge in the meshing tool of the software. A default setting had to be used instead, which prevented the specific settings used in the verification study to be applied.

The default grid settings lead to a grid of 7.6 million cells, recall that this setup is no longer symmetric through the centerline and this would therefore have corresponded to 3.8 million in the verification case (where a grid of 4.3 million cells was preferred). As can be seen in figure for the 4 kts case the bare hull simulations are some $\sim 20\%$ below the test data. Evaluating the results of the verification the following fact can be observed; first, a 20% error would have been predicted for a grid of only 1.6 million cells and then for a grid of 3.8 million cells an error of 12.1% could have been anticipated. This mismatch between results is a consequence of not being able to use the selected grid settings. This also means that the errors of any simulation with the default grid settings can be estimated by the current grid dependence study. The used cell densities are displayed in appendix B.

Deducted from section 1.6.3 there is no test data for the appendage and leeway cases, and as mentioned in section 4.2 there is no verification either. This means that there are no means of evaluating the error in these simulations. As there is no complete series of heel variation, the trends of these series are not available either.

5.2 Trim Variation

The same goes for the trim variations; not enough simulations were finished to draw any conclusion.

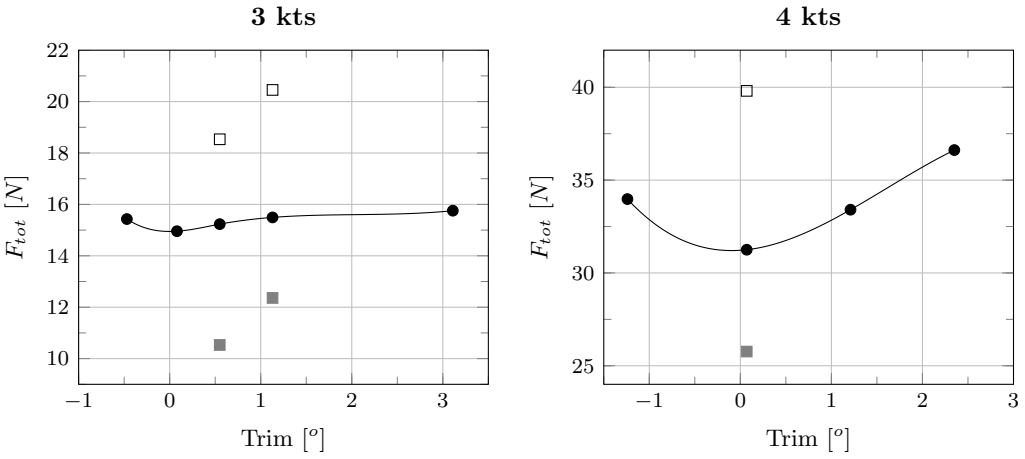

Figure 5.2: Result of trim variation. Positive angle means bow down.
● = Test data; ■ = Bare hull simulations; □ = Appendage and leeway simulations.

6

Concluding Remarks

6.1 Systematic variation of numerical parameters

This section will sum up the study of *systematic variation of numerical parameters*. The study included five different parameters that were expected to have an impact on the predicted resistance of the simulations. These simulations were conducted on grids of 4.5 to 6.5 million cells which turned out to be somewhere at the $\sim 7\%$ plateau (see figure 4.4a).

Density ratio

The result of this study was that the most favorable density ratio was 0.01. The resistance could however be increased by 0.90% by using the physical density ratio but as this lead to very numerically unstable simulations this was not prioritized.

Convergence criteria

This study was done in order to see if uncomplete convergence could be a source of error. The result was that difference in convergence, below the 1% in standard deviation of F_{x_p}, in practice did not affect the result at all.

Domain height

The domain height had a significant effect on the resistance but did also affect the numerical stability of the simulation. Changing the domain height from 0.563 to 0.125 L_{pp} resulted in a decrease of 2.27%. Above 0.536 the simulations became too numerically unstable. As the domain height was $\sim 0.5 L_{pp}$ in the previous simulations already and the threshold of domain height seemed to be 0.536 the positive effect of increased domain height could not be further exploited. The domain height was therefore kept at 0.5 L_{pp}.

Turbulence models

The turbulence models that were implemented for the VOF method in the Shipflow software was EASM and $k\omega - -SST$. The previously used $k\omega$ was clearly superior to the EASM in this case. As the EASM predicted a twice as large error and took substantially more time to converge the $k\omega$ was selected.

Cell density in the transom region

The transom region was refined from the previously used 600 cells per L_{pp}, to 60'000. Only a slight increase in resistance was noticed, 0.51%. This study could however benefit from more thorough investigation as it was discovered that cell densities in other areas of the hull was greatly affected by the transom area. What can be concluded is that an insufficient resolution in the transom area alone, is not a major source of error.

6.2 Investigation

As no conclusion can be made regarding where the major source of this $\sim 7\%$ error lies, at least some numerical parameters can be ruled out by this study. This conclusion will hopefully be useful for future studies of this kind.

The study presented in chapter 4 took the major part of the time of the thesis work. No source for the error was found during this study which meant that the thesis work moved on with a modeling setup that was not accurate. As the objective of this thesis is to find a minima point of a series of heel and trim variations and not necessary an absolute value, it was still considered possible. The setting selected during this study was to be used in the investigation to the largest possible extent. All grid density settings will not be kept completely similar as the investigation will be performed with the boxed grid setup explained in section 3.2.1.

As explained in section 4.2 keeping similar grid settings was not possible. The even keel bare hull case was included in the heel and trim variations but resulted in an even lower resistance than during the verification. As there were larger errors than expected by the grid dependence study the importance of a good grid became even more visible. However as the error for the verification case increased so dramatically during the investigation it can also be concluded that the boxed grid does not perform equally well in this case. This conclusion can be made as the verification case was tested with a non-symmetric H-O-grid as well. The resistance was then 6.9% less than the towing tank test run, compared to the 7.6% of the symmetric case.

7

Future Work

In this section the necessary remaining work to be able to draw conclusions regarding the objective of the thesis will be stated. Also interesting topics for further investigations on this subject will be presented.

Trouble shooting VOF

First of all if the investigation shall be continued using the VOF method in the Shipflow software the source large error for this case has to be found and eliminated. Some possible sources were treated in this thesis but no significant improvement was found.

Complete the heel and trim variations

Another possibility is to use another method entirely to obtain the trim and heel variations. The Shipflow software provides also an inviscid panel method that can be used in combination with a boundary layer method to estimate the viscous part of the resistance. This method was briefly tried during this thesis work to rule out the possibility of having faulty measurement data from the towing tank tests. This was possible because this method is well proven and accepted, unlike the VOF that is a much younger code in this software. It did in that case predict the resistance within a half percent difference from the test data, compared to the best VOF simulation of 6.8%. A positive aspect in using this method is that it is much faster, but it also lacks details of the low. As the appendages and the leeway can be set up for this method as well this is a possible way of obtaining the results.

Simulate the full test matrix

As explained in chapter 5 the current tests are only showing the possible local minima for a trim variation with no heel and a heel variation with no trim. To get the full picture and the global minima in resistance the possibility of combining heel and trim at the same simulation must be investigated. As this will require a substantial amount of time in the towing tank it is not realistic to supply test data for an investigation like this, but with sufficient computational power it would be an interesting study.

Provide sailing instructions

The overall goal with this sports project is to provide sailing instruction to the sailors. As mentioned earlier the hydrodynamic resistance is not the sole key to an optimum sailing technique, there are other aspects that must be taken into account as well.

To get an estimation of the performance of yacht a velocity prediction program, VPP, is used. What this program does is to compute the force and torque balance for the possible degrees of freedom of the yacht, with yaw and trim as exception. The output of the program is then a velocity for a certain apparent angle to the wind for a certain wind speed. The program will then go through a number of wind speeds for a given number of true wind directions, until a graph of the predicted velocities are obtained. The input for the hydrodynamic resistance will be provided by the results of the full test matrix described above, for a range of speeds. The other forces are estimated by empirical formulas. The program will then balance the forces from the sail and thereby obtain a certain heel angle for example. From the data from the VPP the most beneficial angles towards the wind and in terms of heel and trim can then be worked out and presented to the sailors as guide or benchmark.

Investigate actual velocities and attitudes

To limit the amount of simulations needed for the VVP it would be of interest to see which velocities that are achieved on the race track, and what attitudes are used now.

Tailor for individual crew weights

As displayed in section A.2 the change in crew weight has as much as 6% difference in resistance for a case of $\pm 10\ kg$. To really maximize the effect of the individual sailor a separate investigation for the weight of the individual sailor could be performed.

Transient simulation

As mentioned in chapter 5 the representation of the real sailing condition cannot be made more realistic without including time dependent effects. Time dependent phenomena that could be to interest to include in such a simulation is the oncoming waves that are almost always large in comparison to the dinghy. Also the fact that the sailor uses his weight to change the angle of trim to counter wave troughs could be taken into account.

To further more complicate a simulation like this the effect of pumping with boom could be included. The term pumping means here to sheet the main sail to a smaller angle in one quick motion. The purpose of pumping is to generate a burst of power to get the dinghy to water plane on the downwind tacks. A simulation including this maneuver can evaluate how it shall be optimally performed or if it helps at all.

Bibliography

[1] Lars Davidsson. *An introduction to Turbulence Models*. Lecture notes. Chalmers University of Technology, TFD. 2003.

[2] Lars Davidsson. *Numerical Methods for Turbulent Flow*. Lecture notes. Chalmers University of Technology, TFD. 2005.

[3] G. B. Deng, P. Queutey, and M. Visonneau. "Three-dimensional Flow Computation with Reynolds Stress and Algebraic Stress Models". In: *Engineering Turbulence Modelling and Experiments 6* (2005), pp. 389–398.

[4] Luis Eca and Martin Hoekstra. "A procedure for the estimation of the numerical uncertainty of CFD calculations based on grid refinement studies". In: *Journal of Computational Physics* 262 (2014), pp. 104–130.

[5] Luis Eca and Martin Hoekstra. "Discretization Uncertainty Estimation Based on a Least Squares Version of the Grid Convergence Index". In: $2^{nd}WorkshoponCFDUncertaintyAnalysis, Lisabon, October2006$ (2006).

[6] Andreas Feymark. "A Large Eddy Simulation Based Fluid-Structure Interaction Methodology with Application in Hydroelasticity". PhD thesis. Gothenburg, Sweden: Chalmers University of Technology, Shipping and Marine Technology, 2013.

[7] T. B. Gatski and C. G. Speziale. "On explicit algebraic stress models for complex turbulent flows". In: *Journal of Fluid Mechanics* 254 (1993), pp. 59–78.

[8] C.W. Hirt and B D. Nichols. "Volume of Fluid (VOF) Method for the Dynamics of Free Boundaries". In: *Journal of Computaional Physics* 39 (1981), pp. 201–225.

[9] Lars Larsson and Hoyte C. Raven. *Ship Resistance and Flow*. The Society of Naval Architects and Marine Engineers, 2010. ISBN: 9780939773763.

[10] Michal Orych, Lars Larsson, and B Regnstrom. "Adaptive overlapping grid techniques and spatial discretization schemes for increasing surface sharpness and numerical accuracy in free surface capturing methods". In: *28th Symposium on Naval Hydrodynamics Pasadena California USA* (2010), pp. 389–398.

[11] Patrick J. Roache. *Verification and Validation in Computational Science and Engineering*. Hermosa Publishers, 1998. ISBN: 0-913478-08-3.

[12] Christoffer J Roy. "Grid Convergence Error Analysis for Mixed-Order Numerical Schemes". In: *The American Institute of Aeronautics and Astronautics* 41 (4 2003), pp. 596–604.

[13] Christopher Rumsey. *The Menter Shear Stress Transport Turbulence Model*. Web Article. 2013. URL: `http://turbmodels.larc.nasa.gov/sst.html`.

[14] Srdjan Sasic. *Multiphase Flow Lectures*. Lecture notes. Chalmers University of Technology, TFD. 2013.

[15] John W. Slater. *Examining Spatial Grid Convergence*. Web Article. 2005. URL: `http://www.grc.nasa.gov/WWW/wind/valid/tutorial/spatconv.html`.

[16] Fred Stern et al. "Verification and Validation of CFD Simulations". In: *IIHR Report* 407 (1999).

[17] ASME V and V 20 2009. *Standard for Verification and Validation in Computational Fluid Dynamics and Heat Transfer*. The American Society of Mechanical Engineers, 2009. ISBN: 9780791832097.

[18] H. Versteeg and W. Malalasekera. *An Introduction to Computational Fluid Dynamics: The Finite Volume Method (2nd Edition)*. Prentice Hall, 2007. ISBN: 9780131274983.

[19] F. M. White. *Fluid Mechanics (Mcgraw-Hill Series in Mechanical Engineering)*. Science Engineering & Math, 2010. ISBN: 9780073529349.

[20] Lu Zou. "CFD Predictions Including Verification and Validation of Hydrodynamic Forces and Moments on Ships in Restricted Waters". PhD thesis. Gothenburg, Sweden: Chalmers University of Technology, Shipping and Marine Technology, 2012.

[21] Lu Zou and Lars Larsson. “A Verification and Validation Study Based on Resistance Submissions”. In: *Numerical Ship Hydrodynamics, 2010 Workshop* (2010), pp. 203–254.

Appendices

Appendix A

Further Results of the Towing Tank Tests

These results are from the first round of towing tank testing of the Laser dinghy. Concerning the Chalmers sailing project as a whole the Laser will be tested also during a second round when the appendages and leeway will be included in the setup.

As the time in the towing tank booked for the investigation of this thesis allowed more testing than necessary there was time left to look at other effects. First of all the effect of change in crew weight was investigated, and then the effect of using the self bailer device. For the purpose of completion, even as these investigations were not directly associated with the purpose of this thesis, the results of them will hereby be presented.

A.1 Self bailer investigation

The self bailer investigation was done to evaluate the possibility of having increase in resistance due to usage of the self bailing device. The self bailer is a device fitted to the bottom side of the hull in order to evacuate the water from the cockpit. It is able to evacuate water from the dinghy even if that water in the cockpit is below the waterline. This is possible due to the Venturi principle.

The Venturi principle is basically an example of the Bernoulli equation, displaying that the pressure decreases when the velocity of the fluid is increased. In Venturis example the velocity is increased by a decrease in cross sectional area of a pipe, but the principle is also applicable on the nozzle submerged in a flow.

This means that when the nozzle of the self bailer is open, immersed in the flow, it experiences a low pressure created by the faster flow around it. It is therefore self-explanatory that it needs a certain velocity to function properly. The effect of this is displayed in figure A.2: at 6 kts the Venturi effect is large enough even to suck air from the cockpit in under the dinghy, which is made visible by the bubbles. In a racing situation the self bailer will ideally only be used when there is water in the cockpit and these bubbles will therefore not occur.

(a) Open (b) Closed

Figure A.1: Closeup of the self bailer device, seen from underneath.

As this devise has to be lowered into the flow to start working it will thereby create a disturbance on the smooth hull, the resistance will consequently be affected. Figure A.1 shows what the device looks like.

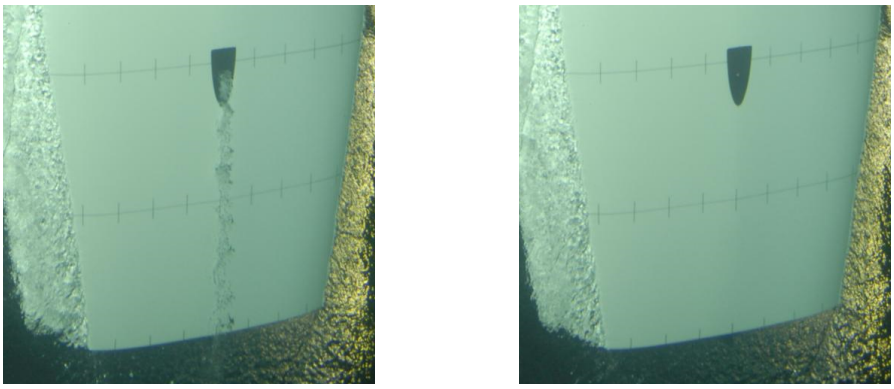

(a) Open (b) Closed

Figure A.2: The self bailer at **6 kts** boat speed.

Concluded from the self bailer investigation is that the self bailer has a small negative impact on resistance. As the boat speed is increased this effect is however more negligible. The results of the test series are presented in table A.1. On the other hand, the opened self bailer will evacuate water from the cockpit and thereby reduce the weight of the boat and decrease the total resistance. Hence the benefits of evacuating the water from the cockpit might overtake the resistance rise due to the open self bailer.

Velocity	Case	F_{tot} $[N]$	Diff	% Increase
4 kts	closed	31.3	0.2	0.64
	open	31.5		
6 kts	closed	112.6	0.6	0.53
	open	113.2		
8 kts	closed	186.7	0.2	0.11
	open	186.9		

Table A.1: Results of self bailer investigation.

A.2 Crew weight investigation

The purpose of this investigation was to quantify the effect of different crew weight in the dinghy. As the Laser is a very strict class rule modifications to the dinghy is out of the question, but there is no restrictions for crew weight. The weight of the sailor naturally affects the total resistance of the boat. For a global view, the total weight of the dinghy with its appendages, rig and equipment is also 80 kg.

In this investigation three crew weights were tested: 70, 80 and 90 kg. The hydrostatics for the three crew weight case can be seen in table A.2. The tests were carried out for a variation of speeds. The dinghy was loaded to obtain even keel at static conditions for all cases. The results of the investigation can be seen in figure A.3.

Case	∇ $[m^3]$	$T_{Lpp/2}$ $[m]$	A_w $[m^2]$	L_{wl} $[m]$
Light	0.150	0.0985	2.806	3.702
Nominal	0.160	0.1022	2.878	3.747
Heavy	0.170	0.1057	2.947	3.793

Table A.2: Hydrostactics data for the three crew weight cases.

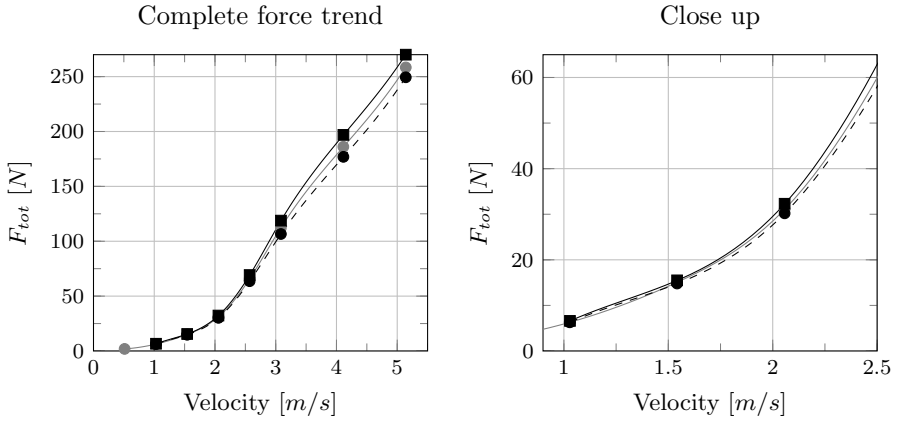

Figure A.3: Crew weight test of total resistance for variation of speeds. Nominal = 80 kg, light = 70 kg, heavy = 90 kg.
■ = Heavy crew (data from series 3); ● = Nominal crew (data from series 1);
● = Light crew (data from series 2).

Concluded from this investigation is that there is a certain advantage in terms of hydrodynamic resistance to have a light weight crew. As seen from the figure A.4, the effect of crew weight is biggest at 3.5 m/s. However there are other aspects to take into consideration when lowering the crew weight. For example a lighter crew will have a reduced capacity of controlling the stability of the boat, the required effort to obtain a certain stability being higher. Therefore during a race it might still be advantageous to have a heavier crew.

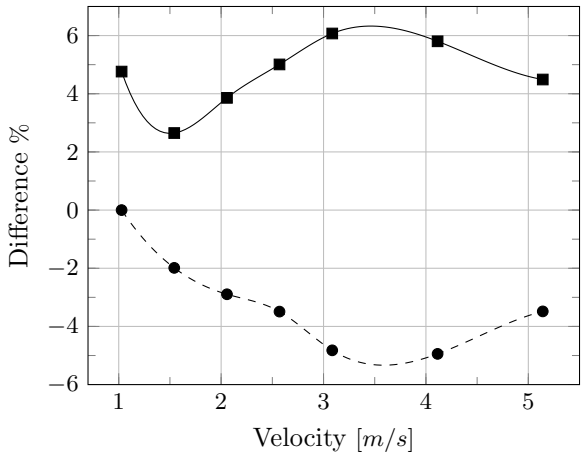

Figure A.4: Precentual difference in total resistance due to change from nominal crew weight.
■ = heavy crew; ● = light crew.

A.3 Trim optimization at zero heel

This section will present a summation of the trim variation investigations performed in series: 5, 6, 7 and 8. To make the results useful as a sailing instruction the following figure shows the trim angle which gives the least resistance at the given velocity.

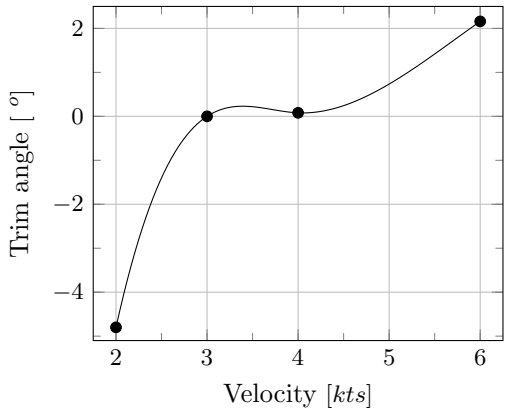

Figure A.5: Angle of trim resulting in minimum resistance for a varation of speed. Positive angle means bow up.

To have in mind when evaluating this figure is that the minima obtained at the different velocities are for sailing a zero degrees heel and leeway angle. This means that it can be interesting for downwind sailing. The tests did neither account for the effects of oncoming waves. As it might be beneficial for downwind sailing to also include the troughs of the waves to gain speed, these results shall be viewed with caution.

Appendix B

Zonal Cell Densities

Region (direction)	Verification (*grid* 2)	Investigation
Upstream (longitudinal)	51	140
Bow (longitudinal)	168	280
Midships (longitudinal)	90	127
Transom (longitudinal)	1010	1600
Wake (longitudinal)	101	476
Overall (radial)	42	160
y_1^+	0.7	1.0

Table B.1: Comparison of cell densities at different regions. Densities expressed in cells per L_{pp}, y^+ is expressed in dimensionless length unit.